Check for updates

RESEARCH ARTICLE SUMMARY

DRUG DISCOVERY

Discovering molecular modulators with nanoswitch screening

Clinton H. Hansen†, Mark Lipstein†, Sarah C. Erlandson, Tobias Schwalbe, Sylvie G. Bernier, Peter Gmeiner, Andrew C. Kruse, Wesley P. Wong*

Full article and list of author affiliations: https://doi.org/10.1126/science.adt7185

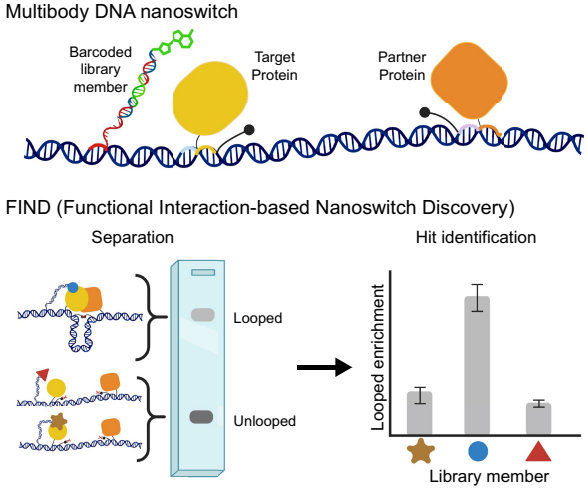
INTRODUCTION: Protein-protein interactions are central to nearly all biological processes and play critical roles in disease. Molecules that modulate these interactions, either by bringing specific proteins together or by stabilizing beneficial protein conformations, have emerged as key therapeutics. Yet these molecular modulators can be challenging to discover, as standard screening approaches often lack throughput or fail to directly assay multibody interactions. Thus, combining the scale of nucleotide-encoded libraries with direct selection for desired interaction outcomes could accelerate the discovery of therapeutics for a wide range of conditions.

RATIONALE: To address these challenges, we developed FIND (Functional Interaction–based Nanoswitch Discovery), a platform for discovering compounds that induce or increase protein-protein interactions. FIND combines DNA nanoswitch–based selection of nucleotide-encoded libraries with next-generation sequencing, enabling ultra-high-throughput screening of billions of different compounds in parallel in a single-pot experiment. Self-assembled nanoscale devices called "DNA nanoswitches" physically link proteins of interest to candidate molecules on a DNA scaffold. When a compound promotes or stabilizes a protein-protein interaction, the scaffold switches from a linear to a looped conformation. Looped nanoswitches migrate more slowly than linear ones during gel electrophoresis, enabling physical separation. The compounds linked to these looped nanoswitches are then identified by sequencing their DNA barcodes. This approach enables direct selection of molecules on the basis of their ability to induce specific protein-protein interactions, rather than simply on the basis of their binding to proteins.

RESULTS: We demonstrated the ability of FIND to discover new compounds from large libraries with two distinct applications. First, we discovered a nanobody (single-domain antibody) that stabilizes the interaction between angiotensin-converting enzyme 2 (ACE2) and the spike trimer of severe acute respiratory syndrome coronavirus 2 (SARS-CoV-2). This stabilizing nanobody also showed activity in a cellular infection assay. Such molecules can be valuable research tools for understanding how antibodies and other binding proteins influence interactions between virus and host receptors, including in the phenomenon of antibody-dependent enhancement. The second example focused on small-molecule discovery against an intracellular target. Specifically, we screened a DNA-encoded library of small molecules to discover activators, or agonists, of peroxisome proliferator–activated receptor gamma (PPARγ), a regulator of metabolism and target for diabetes therapy. FIND identified novel small molecules that increased the binding of PPARγ to a coactivator peptide. These hits were validated in biochemical assays and increased lipid accumulation in a cellular assay.

CONCLUSION: FIND is a broadly adaptable ultra-high-throughput screening platform that can identify molecules capable of modulating protein-protein interactions. By directly selecting for functional interaction outcomes, FIND expands the capabilities of the traditional screening toolbox, enabling rapid discovery of molecular modulators, which could accelerate therapeutic development across many conditions. □

*Corresponding author. Email: wesley.wong@childrens.harvard.edu †These authors contributed equally to this work. **Cite this article as C. H. Hansen *et al.*, *Science* 394, eadt7185 (2026). DOI: 10.1126/science.adt7185**



Principles of FIND for selecting molecular modulators. DNA nanoswitches incorporate a target protein, its partner protein, and a barcoded library member on a DNA scaffold. When a library member promotes interaction between two proteins of interest, the DNA nanoswitch forms a loop. Gel electrophoresis separates looped from unlooped nanoswitches, enriching loop-inducing compounds, which are identified by sequencing their DNA barcodes. [Figure created with BioRender.com (2026); https://BioRender.com/p6c3nwh]

Downloaded from https://www.science.org at Harvard University on November 05, 2026

DRUG DISCOVERY

Discovering molecular modulators with nanoswitch screening

Clinton H. Hansen[1,2,3]†, Mark Lipstein[1,3,4]†, Sarah C. Erlandson[5], Tobias Schwalbe[6], Sylvie G. Bernier[3], Peter Gmeiner[6], Andrew C. Kruse[5], Wesley P. Wong[1,2,3,5]*

Molecules that modulate protein-protein interactions, including through ternary complex formation, have been established as key therapeutics. Yet they can be challenging to discover, as standard screening approaches often lack throughput or fail to directly assay multibody interactions. We addressed this by combining DNA nanoswitch–based selection of nucleotide-encoded libraries with next-generation sequencing to create FIND (Functional Interaction–based Nanoswitch Discovery), which enables ultrahigh-throughput discovery of compounds that induce or increase protein-protein interactions. We demonstrate FIND by discovering nanobodies that stabilize the interaction between angiotensin-converting enzyme 2 and the receptor-binding domain of severe acute respiratory syndrome coronavirus 2 and by discovering agonists of peroxisome proliferator–activated receptor gamma from a DNA-barcoded small-molecule library. By enabling rapid discovery of molecular modulators, FIND could lead to new therapeutics across many conditions.

Protein-protein interactions have key roles in virtually all biological processes. Molecules that modulate protein-protein interactions, either by mediating ternary complex formation or by allosterically stabilizing specific protein conformations, have emerged as important therapeutics for many diseases (*1*, *2*). Such compounds include salbutamol used to treat asthma (*3*), semaglutide used to treat diabetes (*4*), cystic fibrosis transmembrane conductance regulator modulators used to treat cystic fibrosis (*5*), and thalidomide used to treat cancer (*6*). Yet such molecules can be challenging to discover, because standard screening approaches often lack either the throughput or the functional readout required to efficiently find modulators of multiprotein interactions. Plate-based assays can in principle identify interaction modulators, but compounds are typically tested individually in separate wells, limiting throughput. Even with miniaturization and automation, such screens remain resource-intensive and typically test 10^5 to 10^6 compounds, reducing the probability of discovering rare modulators (*7*). DNA-encoded libraries (DELs) enable screening of far larger chemical spaces (of up to ~10^{12} members) through pooled affinity selections and sequencing-based barcode readouts, but standard DEL selections typically enrich for binders to immobilized protein targets rather than compounds that promote or stabilize specific multiprotein interaction states (*8*). For targeted degradation, induced-proximity approaches such as proteolysis-targeting chimeras (PROTACs) highlight the therapeutic power of ternary complexes—although even within this focused scope, PROTAC development typically requires starting ligands for both partners and substantial iterative optimization of the linked construct (*9*). Thus, combining the scale of nucleotide-encoded libraries with direct selection for desired interaction outcomes could accelerate the discovery of therapeutics for a wide range of conditions.

One potential avenue to accomplish this is through DNA nanotechnology, which enables the development of programmable biomolecular reagents that sense, probe, and report on molecular interactions (*10*–*15*). In fact, DNA scaffolds can investigate ternary interactions by positioning candidate binding partners at defined locations and enabling a measurable readout when a third molecule induces binding. This readout can be achieved using Förster resonance energy transfer (FRET) on Y-shaped DNA scaffolds (*16*), altered gel migration due to DNA loop formation (*14*, *17*), or changes in tether motion or extension measured by single-molecule tethered particle motion or magnetic tweezers assays (*17*–*19*). If an ensemble of such nanoscale devices could complement or partially replace traditional robotic plate handlers, this approach might offer the scale and analytical power needed to empirically identify rare molecular modulators directly from large libraries. To achieve this, we combined structural DNA nanotechnology with nucleotide-encoded libraries to create FIND (Functional Interaction–based Nanoswitch Discovery), a platform for logic-gated compound selection based on defined interaction outcomes, such as induction or stabilization of protein-protein interactions, or allosteric modulation of pharmacologically relevant targets. The basis of FIND is the DNA nanoswitch (*14*, *20*), a programmable molecular scaffold that switches between linear and looped conformations to report interactions between attached components, such as proteins or small molecules. Specifically, binding proteins are coupled to oligonucleotides that hybridize to defined locations along a linear DNA strand, which forms loops if the proteins interact. This change in topology allows separation of nanoswitches with different looped and unlooped configurations by gel electrophoresis, as looped nanoswitches migrate more slowly through the gel than unlooped, linear nanoswitches. By attaching multiple interaction partners to each nanoswitch, we can construct an in vitro assay that measures how compounds modulate a target protein's binding to specific interaction partners (Fig. 1A). The programmable self-assembly of nanoswitches enables precise control over the number, stoichiometry, and spatial organization of components on each scaffold by allowing researchers to specify which molecules are attached and how far apart they are positioned along the DNA strand, setting their effective local concentrations. Together, these capabilities enable nanoswitch assays that directly report whether a compound promotes specific multiprotein interactions, providing a broadly adaptable strategy for characterizing and discovering modulators, such as allosteric activators, protein-protein interaction enhancers, and potentially also molecular glues (Fig. 1B). We also adapted a latching system to enable FIND to assay weak interactions (Fig. 1C).

FIND enables ultrahigh-throughput functional selection of nucleotide-encoded libraries by coupling pooled nanoswitch assays to next-generation sequencing. In this combined workflow, the nanoswitch assay provides selection based on interaction outcomes, while nucleotide encoding and sequencing provide the scale. Each nanoswitch is linked to a library member carrying a different nucleic acid barcode that can be read out by sequencing, enabling testing of billions of different compounds in parallel in a single-pot experiment. These libraries can include DELs for small molecules, in which each compound is physically linked to a DNA barcode that records the series of chemical synthesis steps used to build it (*8*), and mRNA display libraries for biologics (*21*). To perform selection, library-functionalized nanoswitches containing proteins of interest are separated by gel electrophoresis into looped and unlooped fractions. Thus, selection is directly based on whether the library member promotes a specific interaction outcome, such as by induction or stabilization of the desired protein-protein interaction (Fig. 1D). Each nanoswitch thus serves as an independent assay compartment,

[1]Program in Cellular and Molecular Medicine, Boston Children's Hospital, Boston, MA, USA. [2]Department of Pediatrics, Harvard Medical School, Boston, MA, USA. [3]Wyss Institute for Biologically Inspired Engineering, Harvard University, Boston, MA, USA. [4]Biological and Biomedical Sciences Program, Harvard Medical School, Boston, MA, USA. [5]Department of Biological Chemistry and Molecular Pharmacology, Blavatnik Institute, Harvard Medical School, Boston, MA, USA. [6]Department of Chemistry and Pharmacy, Friedrich-Alexander University Erlangen-Nürnberg, Erlangen, Germany. ***Corresponding author. Email: wesley.wong@childrens.harvard.edu** †These authors contributed equally to this work.

Downloaded from https://www.science.org at Harvard University on November 05, 2026

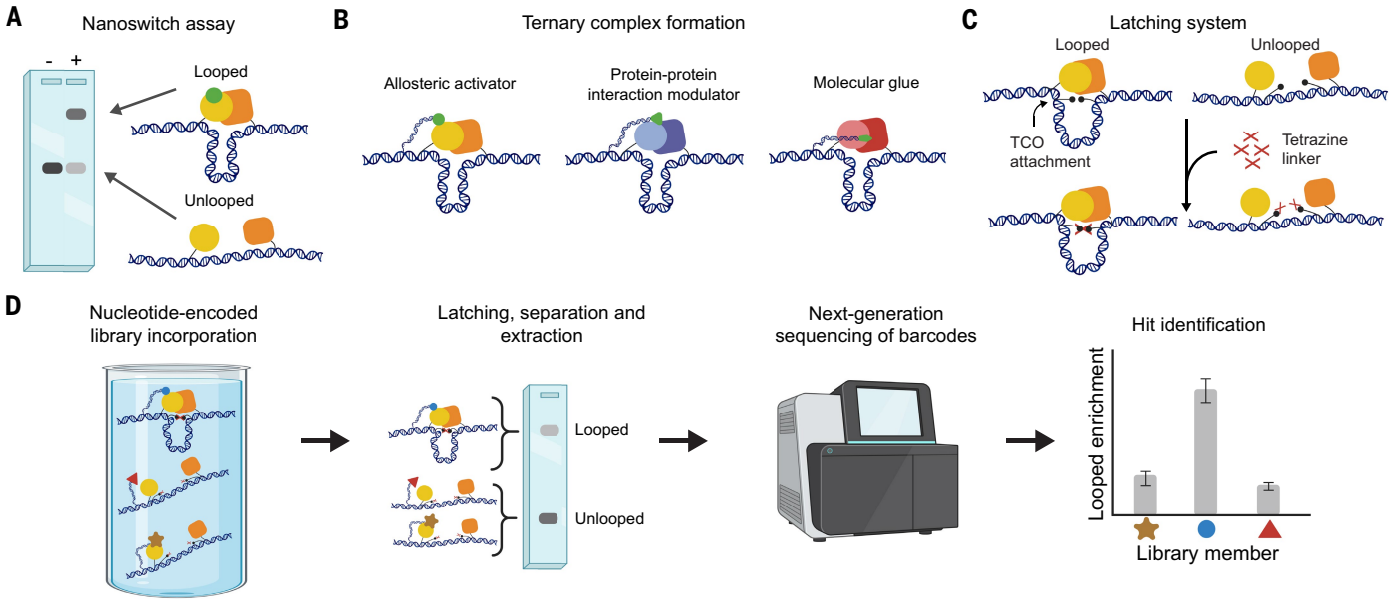


Fig. 1. Functional Interaction–based Nanoswitch Discovery (FIND). (**A**) DNA nanoswitches are created by attaching target proteins to a linearized M13 DNA scaffold by oligonucleotide coupling followed by hybridization. Interactions between the proteins change the topology of the strand from a linear to a looped conformation, resulting in reduced migration during gel electrophoresis. (**B**) Nanoswitch assays can be used to detect attached compounds that promote ternary complex formation. The molecular glue example illustrates a potential application beyond those demonstrated here. (**C**) Latching system for stabilizing weakly looped nanoswitches before gel-based separation. Each construct has two TCO groups near the attached proteins, and latching occurs after incubation by addition of bifunctional tetrazine linkers, which covalently stabilize the looped population before gel loading. For looped constructs, once one TCO binds to the tetrazine linker, the local concentration of the other TCO is high, and it quickly binds to the other end of the linker. For unlooped constructs, because the TCO groups are farther apart on average, both TCO groups are more likely to bind to different linkers, resulting in no loop-stabilizing latch. (**D**) An example of a FIND screen for activators from a nucleotide-encoded library that cause two proteins to interact. The barcoded library is incorporated onto the nanoswitch, along with the protein targets. Next, nanoswitches are separated into looped and unlooped fractions on an agarose gel. Then the bands are extracted and quantified by high-throughput DNA sequencing. Potential activators are identified by an increase in the frequency of their barcode sequences in the looped band compared with the unlooped band. [Figure created with BioRender.com (2026); https://BioRender.com/wes71vh]

enabling multiplexed selections in a single pooled reaction that identify modulators of multiprotein complexes rather than compounds selected solely for binding to a target. Because interacting components are maintained at high local concentrations on each nanoswitch, FIND facilitates detection and characterization of weak interactions that could otherwise be challenging to identify in traditional bulk assays.

In the next section, we describe the basic design principles of FIND and demonstrate the workflow using a DNA model system. We then apply FIND to three protein-based systems: enrichment of G protein–coupled receptor (GPCR) agonists from a spike-in library, discovery of biologic modulators of the interaction between severe acute respiratory syndrome coronavirus 2 (SARS-CoV-2) spike protein and its human receptor angiotensin-converting enzyme 2 (ACE2), and discovery of peroxisome proliferator–activated receptor gamma (PPARγ) agonists from a small molecule DEL.

FIND workflow and design principles: Stem-loop model system

To implement FIND, DNA nanoswitches were created by hybridizing oligonucleotides attached to molecules of interest onto an M13 DNA scaffold, positioning them at defined locations (Fig. 2A and fig. S1). Each nanoswitch included the interaction partners of interest together with a single barcoded library member, identifiable by its specific nucleic acid sequence. Binding between molecules attached to the same nanoswitch caused the formation of loops, which reported desired interaction outcomes. Covalent latches were added to stabilize looped configurations (fig. S2), and the loops were separated from the unlooped nanoswitches by gel electrophoresis. These fractions were extracted, and the attached barcodes were sequenced to quantify enrichment. Because each nanoswitch carried at most one library member and adopted a discrete (looped or unlooped) topology, the assay was effectively digital in terms of single molecules even though the readout was quantified in bulk by sequencing.

To demonstrate and characterize this process, we implemented FIND in a nucleic acid model system built around a DNA stem-loop that functions as a simplified "receptor" (fig. S1A). In this system, short DNA sequences that act as "ligands" bind a 6-nucleotide (nt) toehold region of the DNA stem-loop, causing it to open and bind to a complementary DNA sequence on the nanoswitch that acts as a binding partner. In this way, the stem-loop system acts like a protein-receptor cognate that can be activated to increase binding to a downstream partner. Specifically, opening of the stem-loop enabled it to bind to a 10-nt complementary downstream sequence spaced 1458 nt away on the nanoswitch, which created a large loop for gel separation. As an initial validation of this model system, a perfectly matching opening ligand sequence containing the full 6-nt complement to the toehold region produced an up to 70-fold increase in looped-band intensity relative to a library of random toehold sequences (fig. S3A).

Several design considerations determine FIND performance for a given molecular system. Because some interactions of interest may not be strong enough to stably hold together a nanoswitch loop during gel electrophoresis, we incorporated a molecular latch into the nanoswitch construct that covalently stabilized looped nanoswitches by click-chemistry, essentially locking in the distribution of looped and unlooped nanoswitches present in the reaction mixture before gel loading (Fig. 1C and fig. S2). Unless otherwise noted, we used this latching step for all library screening assays. To implement this, each nanoswitch included two *trans*-cyclooctene (TCO)–modified latch oligonucleotides

Downloaded from https://www.science.org at Harvard University on November 05, 2026

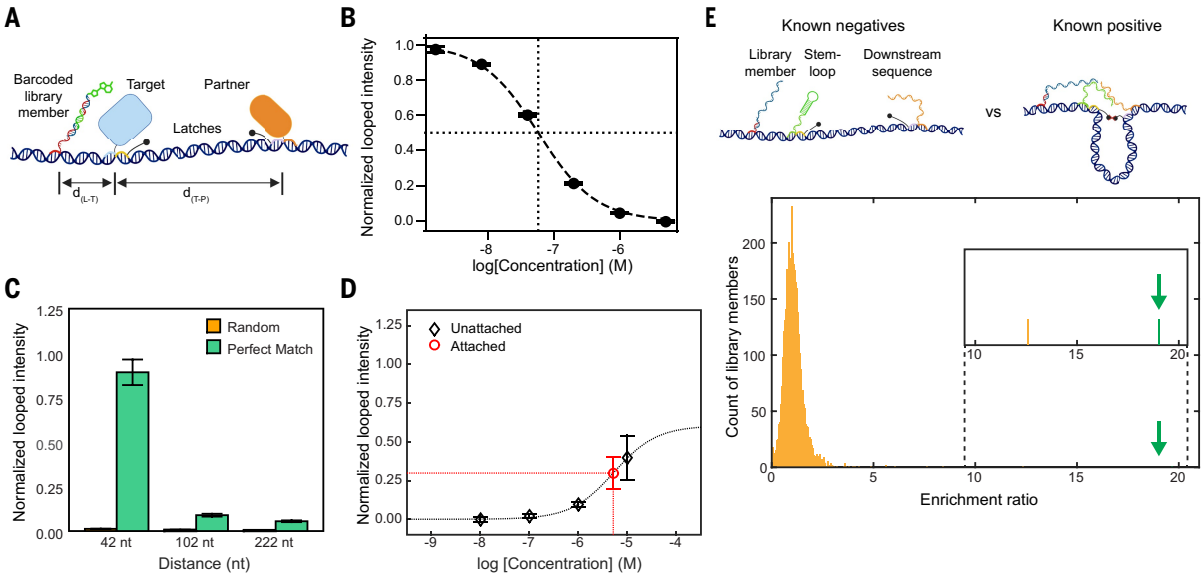


Fig. 2. FIND design principles and multiplexed stem-loop selection. (**A**) Schematic of FIND screening on DNA nanoswitches (not to scale). Barcoded library members are hybridized to the scaffold (M13 ssDNA), through direct binding or a capture oligonucleotide. "Partner" and "target" molecules are functionalized with oligonucleotides bearing flexible PEGylated linkers, alongside adjacent TCO latch-modified oligonucleotides for latching. [Panel created with BioRender.com (2026) https://BioRender.com/956coyq] (**B**) Competition of the stem-loop system with a free, unbound oligonucleotide that binds to the attached "partner" oligonucleotide with the same number of complementary nucleotides as an open stem-loop ($N = 4$, SEM). The measured effective local concentration on the nanoswitch between the "target" and "partner" is the $IC_{50} = 58$ nM. (**C**) Normalized looped intensities for stem-loop binding to target oligonucleotide after binding to either a perfectly matched library member or to a random sequence (in the toehold region) spaced a certain number of nucleotides away ($N = 4$, SEM). The library member has a 6-nt toehold-binding region and a constant 5-nt region complementary to the stem region. (**D**) Normalized dose-response curve for stem-loop opening by a 9mer oligonucleotide with four nucleotides complementary to the toehold region and five nucleotides complementary to the stem region of the stem-loop ($N = 4$, SEM). A sigmoidal fit (black dashed line) yields $EC_{50} = 5.3 \times 10^{-6}$ M (2.2×10^{-6}, 1.1×10^{-5}) and $E_{max} = 0.60$ (0.31, 1.14), with 95% confidence intervals. Also shown is the signal from the same sequence when attached to the nanoswitch (red) and the deduced effective local concentration between the attached library member and the stem-loop target receptor, 5.1×10^{-6} M, determined by matching this signal to the dose-response curve (red dashed lines). (**E**) Results of a multiplexed selection for agonist DNA sequences that can bind to and subsequently open a stem-loop with a toehold, activating the stem-loop to bind a target oligonucleotide, leading to formation of looped nanoswitches. For each of the 4096 different toehold sequences, an enrichment ratio was calculated as the ratio of normalized sequencing reads in the looped band to those in the unlooped band; the histogram shows the number of library members at each enrichment ratio. Here, sequences that directly bind to the target complementary sequence are filtered out by performing an additional sequencing experiment without the stem-loop to find members that bind with an enrichment of >1.5. The perfect complementary match (green arrow) is higher than all other sequences, with a P value of 1.1×10^{-9} over the background using a one-sided z-test of log(enrichment). [Top panel of (E) created with BioRender.com (2026); https://BioRender.com/0w1u0yh]

positioned near the interaction sites; latching was initiated by adding a bifunctional tetrazine cross-linker (Figs. 1C and 2A and fig. S2). In the looped configuration, the two reactive handles are brought into proximity, which creates a high effective local concentration that favors rapid intramolecular cross-linking, whereas in the unlooped configuration the handles are predominantly end-capped by separate cross-linkers, which suppresses background latching.

The spacing between the primary interaction partners [the target receptor and its partner, labeled as $d_{(T\text{-}P)}$ in Fig. 2A] on the DNA scaffold was selected to balance two competing requirements: It needed to be large enough to enable clear separation between looped and unlooped nanoswitches by gel electrophoresis, yet small enough to maintain a sufficiently high effective local concentration for strong binding upon activation and a strong signal. For this model system, we experimentally quantified the effective local concentration between the nanoswitch receptor and partner by performing a competition assay with a free oligonucleotide that blocked binding between the DNA stem-loop receptor and its partner attached to the nanoswitch, preventing loop formation (Fig. 2B) (*14*, *22*). In this way, the concentration of free oligonucleotide that reduced the looped intensity to 50% of maximum corresponded to the effective concentration between the nanoswitch partners, or concentration of equal competition. We measured the normalized intensity of the looped band by first subtracting the background intensity, then dividing by the background-subtracted looped-band intensity measured in the absence of any blocking oligonucleotide (fig. S3B). We measured the effective local concentration between the target receptor and its partner to be 58 nM, on the basis of their locations in the stem-loop model system. If necessary, this effective concentration could be further tuned to better match the dissociation constant (K_d) of an interaction of interest by changing the distance $d_{(T\text{-}P)}$ between binding partners on the DNA scaffold, as governed by polymer physics. Overall, these readily accessible effective concentrations enabled the nanoswitch to measure changes in binding strength for interactions with affinities in the nano-to-micromolar range. The tether between binding partners must also be long enough and flexible enough for binding to occur. We used flexible linkers to connect proteins to the DNA scaffold and to ensure that the distance on the scaffold between binding partners was long enough (many persistence lengths) to provide sufficient translational and orientational flexibility.

For multiplexed ligand screening, the library member itself must be tethered close enough to the receptor to achieve sufficiently high local concentration for weakly binding ligands [this distance is labeled as $d_{(L\text{-}T)}$ in Fig. 2A]. The tiling area between the library member attachment and target also contains single-stranded regions for increased flexibility (fig. S1B). DNA library sequences contained a 6-nt toehold-binding region, a constant 5-nt region complementary to the targeted stem-loop, and a constant sequence to bind to a capture oligonucleotide

Downloaded from https://www.science.org at Harvard University on November 05, 2026

on the nanoswitch. Positioning the library member via a capture oligonucleotide located 42 nt from the DNA stem-loop "receptor" produced a stronger looping signal than positioning it farther away, at 102 or 222 nt (Fig. 2C). To determine the effective local concentration between the library member "ligand" and the stem-loop "receptor," we compared the looped-band intensity produced by a nanoswitch-attached library member with the intensity produced by the same ligand free in solution at different concentrations. For this nanoswitch geometry, matching the attached-ligand signal to the free ligand dose-response curve yielded an effective local concentration of 5.1 μM between the attached library member and the target receptor (95% confidence interval of 3.0×10^{-6}, 9.9×10^{-6}) (Fig. 2D and fig. S3C). Thus, this geometry enabled characterization of weakly binding ligands with affinities in the low-micromolar range. As long as the effective local concentrations between molecules linked to a single nanoswitch was higher than the bulk solution concentrations of these components, they were more likely to interact with each other than with other components in the solution (e.g., intrascaffold interactions were favored over interscaffold interactions).

With these design parameters established, we used this stem-loop system to demonstrate the full FIND workflow in a pooled, highly multiplexed, sequencing-based screen. We performed multiplexed selection using a starting library containing all random 6-nt toehold sequences and quantified enrichment for each sequence with high-throughput sequencing. For each library member, we calculated the enrichment as the number of reads in the looped band over the number of reads in the unlooped band, each normalized by the total number of reads. To filter out library member sequences that could directly bind to the downstream sequence, we performed a parallel experiment for nanoswitches with no stem-loop. We used the resulting sequencing data to filter out library members that bound directly to the complementary downstream sequence by identifying sequences that were enriched >1.5 times over the background. This filtering was a special case that should not usually be needed, but in this experiment, certain library members bound more strongly to the complementary downstream sequence than any members bound to the stem-loop owing to competition with secondary structure in the stem-loop.

The sequence with the perfect complement to the toehold had the highest enrichment, 18 times [one-sided z-test of log(enrichment), $P = 1.1 \times 10^{-9}$] over the background (Fig. 2E). Similarly, when we averaged over sequences with nonbinding nucleotides at the end of the toehold region, perfect matches for 3, 4, and 5 nt had enrichments of 1.7355 ($P = 5.0 \times 10^{-4}$), 1.8304 ($P = 3.1 \times 10^{-3}$), and 7.6428 [$P = 2.4 \times 10^{-10}$, one-sided z-test of log(enrichment)], respectively, over the background (fig. S3D). Increasing complementarity led to increasing enrichment, demonstrating that a single multiplexed nanoswitch assay can both find low affinity library members that act as agonists and also determine their relative strengths.

FIND validation for GPCR ligand enrichment and profiling

To validate the use of FIND with pharmacologically relevant protein targets, we used it to enrich a known agonist of the β_2-adrenergic receptor (β_2AR), a GPCR, from a model DEL of small molecules containing one agonist among DNA-barcoded controls (Fig. 3). GPCRs are major pharmaceutical targets (*23*), yet current methods for discovering and profiling pathway-activating ligands often rely on material-intensive in vitro assays (*24*) or cell-based reporters (*25*–*28*). Thus, efficient and accessible multiplexed screening approaches such as FIND could be of benefit.

Before incorporating nucleotide-encoded libraries of small molecules for screening, we validated study of ternary complex interactions in GPCRs, in an assay with two components attached to the nanoswitch and a third component in solution modulating their interaction. We characterized the interaction between a GPCR and a biomolecule

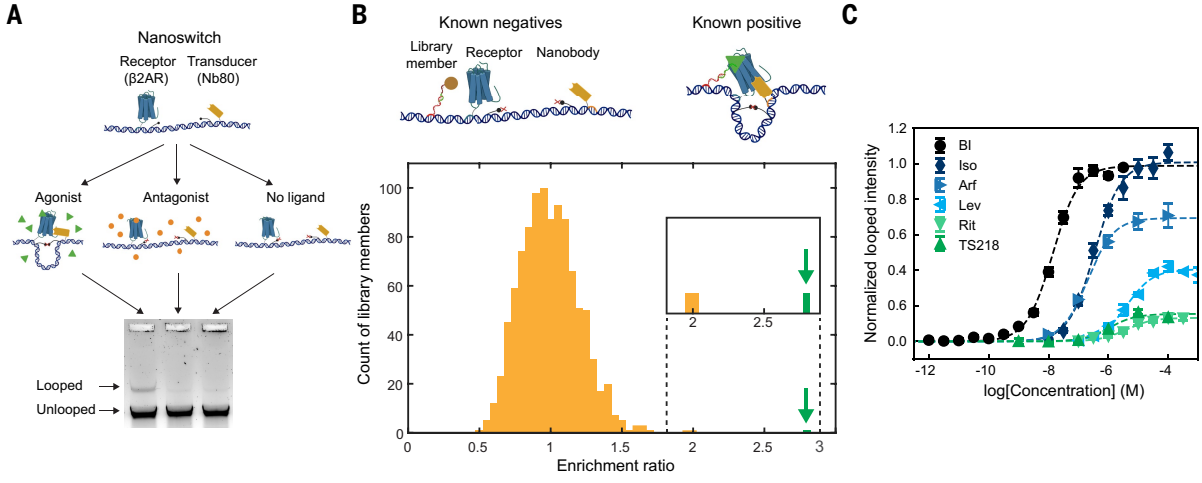


Fig. 3. FIND for multiplexed selection and characterization of GPCR ligands. (**A**) DNA nanoswitches created by hybridizing protein-oligonucleotide conjugates of the β_2AR and the G protein transducer mimic nanobody, Nb80, along with tiling oligonucleotides onto a linearized M13 scaffold. Incubating 100 pM nanoswitches with an agonist activated the receptor, which increased the amount of looped nanoswitches through increased receptor-nanobody binding, leading to a looped band observed during gel electrophoresis. Conversely, incubating with an antagonist or in the absence of ligand did not cause an increase in looped band intensity. [Created with BioRender.com (2026); https://BioRender.com/wg15nzz] (**B**) Results of a multiplexed selection for agonists of β_2AR using nanoswitches that each carried β_2AR, Nb80, and one member from a model library containing a known partial agonist. DNA-barcoded library members were added as single-stranded oligonucleotides and hybridized to the capture site during nanoswitch assembly. The enrichment of counts in the looped band over the unlooped band is shown for a library in which the DNA-barcoded compounds consisted of 1 positive control DNA sequence bound to TS218 and 1024 DNA negative control sequences bound to biotin. The positive control (green arrow) has an enrichment of counts in the looped band over the unlooped band higher than all the negative controls, with a P value of 1.4×10^{-7} using a one-sided z-test. [Created with BioRender.com (2026); https://BioRender.com/oc88xcu] (**C**) Normalized dose response curves of the agonists using DNA nanoswitches. The response at each dose was given by the looped band intensity, which we quantify by integrating the area under the curve of the looped band, subtracting the background, and normalizing to the BI maximal response ($N = 4$, SEM). Fit values to a sigmoidal response (dashed lines) are given in table S1. BI, BI-167107; Iso, isoprenaline; Arf, arformoterol; Lev, levosalbutamol; Rit, ritodrine.

Downloaded from https://www.science.org at Harvard University on November 05, 2026

that mimics the G protein transducer (a "transducer-mimic") in the presence of various ligands. By attaching both a GPCR and a transducer-mimic to nanoswitches, we read out the functional state of the GPCR bound to different ligands to determine drug characteristics, such as affinity and activity. We used β_2AR and a G protein mimic nanobody, Nb80, that binds to active-state β_2AR (*29*). As GPCRs are membrane proteins, we added 0.01% lauryl maltose neopentyl glycol (LMNG) and 0.001% cholesteryl hemisuccinate (CHS) to solubilize β_2AR in detergent micelles. To construct the DNA nanoswitches, we coupled β_2AR and Nb80 to short oligonucleotides and hybridized them onto locations on the single-stranded scaffold. We used latching to stabilize the interaction (fig. S4A). To demonstrate that nanoswitches measured the functional state of β_2AR, we determined the amount of looping in the presence of agonist BI167,107 (BI) or the inverse agonist ICI 118,551 (ICI) and in the absence of any ligand (Fig. 3A). The looped band increased in intensity in the presence of agonist, indicating activation of β_2AR and its resultant binding to Nb80.

Having demonstrated that agonists induced binding between β_2AR and Nb80 tethered to the nanoswitch, we tested enrichment of agonists in a model library screen. As in the stem-loop experiments, we constructed nanoswitches with an oligonucleotide to capture DNA-barcoded small molecules, in addition to the receptor and nanobody. The capture oligonucleotide has deoxyinosine over variable bases and deoxyuridine instead of deoxythymine for cleavage before sequencing preparation. As an example, we used 1024 DNA sequences attached to biotin and a single sequence attached to the partial agonist TS218 (figs. S4B and S5), a structural analog to covalent adrenaline derivatives (*30*, *31*). These sequences mimicked those of a macrocycle library (*32*). The sequence corresponding to TS218 was the most highly enriched sequence above the background ($P = 1.4 \times 10^{-7}$, one-sided z-test) (Fig. 3B). This enrichment in the looped fraction occurred even though the overall abundance of TS218 input into the selection is not highly enriched compared with other sequences (fig. S4C). In a nonmultiplexed experiment, we confirmed that TS218 attached to the nanoswitch resulted in a signal above the background (fig. S4D). Conversely, the attached antagonist BRL37344 (*33*) did not result in a signal above the background (fig. S4D), even though attached BRL37344 can form loops with β_2AR when placed 1458 nt away (fig. S4E).

We used our nanoswitch reagent to characterize the dose-response curve for TS218 (Fig. 3C). Each curve defined the two key pharmacological parameters of the agonist: its potency [half-maximal effective concentration (EC_{50}); related to agonist affinity] and its efficacy (E_{max}; related to the degree of activation when the agonist is saturating). TS218 had an EC_{50} for looping of 1.1 μM, which is of a similar order of magnitude to EC_{50} values reported for β_2AR agonists and partial agonists measured in intact-cell cyclic adenosine monophosphate assays (nano-to-micromolar range) (*34*). We also used this approach to gather dose-response curves for various other agonists (Fig. 3C). Full agonists (BI167107, isoprenaline, and arformoterol) had higher looping percentages at saturation than did partial agonists (levosalbutamol and ritodrine), providing a straightforward and quantitative measure of relative molecular efficacy without confounding effects such as signal amplification. To further demonstrate the versatility of our assay, we characterized antagonists in a competition assay with the partial agonist levosalbutamol (fig. S4F) and performed dose-response experiments with a mini-G protein corresponding to the engineered Ras-like domain of Gα subunits (*35*, *36*) instead of a nanobody (fig. S4G). We also used the nanoswitch assay to profile the functional states of β_2AR bound to various ligands (supplementary text and figs. S6 and S7).

Discovery of a SARS-CoV-2 protein-protein interaction enhancer

To demonstrate the power of FIND to help discover modulators from a naïve library, we selected for nanobodies that enhanced the interaction between the SARS-CoV-2 spike trimer and its receptor, ACE2. Interaction-enhancing binders are of particular interest because infection-enhancing antibodies have been described for SARS-CoV-2 and understanding how such reagents can increase receptor engagement can provide insight into antibody-dependent enhancement (ADE) mechanisms that could promote viral entry in the context of COVID-19 (*37*, *38*). Additionally, molecular stabilizers can serve as useful experimental tools for probing the conformation-dependent energetics and kinetics of this interaction and for tuning binding strength in model systems where native receptor binding may be suboptimal (*39*). To perform the screen, we started with a nanobody mRNA display library of ~20 billion members that was constructed in a similar manner to a previous yeast display library (*40*), which we then enriched by a traditional bead-based selection protocol (methods). For nanoswitch-based screening, we attached ACE2, the spike trimer, and a member of the enriched nanobody library to each DNA scaffold. The mRNA-displayed nanobody was attached to the nanoswitch through a DNA adapter that contained both the reverse-transcription primer sequence from the library and an overhang that was the reverse-complement of a sequence on the nanoswitch scaffold. Overnight incubation of the nanoswitch with the displayed nanobody enabled attachment (fig. S8A) without degradation (fig. S8B). Using FIND, we discovered a particular nanobody (Nb1) that stood out with significant enrichment above the background (Fig. 4A; generalized extreme Studentized deviate test $P = 9.0 \times 10^{-9}$). FIND results were reproducible, as demonstrated by the low SEM and spread of the enrichment ratios across the three replicates (fig. S8C). Nb1 also had the highest enrichment ratio for two other independent replicates of the nanoswitch screen (fig. S8D). Nb1 had the highest enrichment ratio, even though it was not the top by abundance through bead-based enrichment (fig. S8E).

To confirm and quantify the effect of Nb1 on the interaction between ACE2 and the spike trimer, we expressed the Nb1 nanobody and incubated it with nanoswitches that only included ACE2 and the spike trimer on the scaffold. The amount of looping increased in the presence of Nb1 because of increased binding between the ACE2 and spike trimer, but did not increase with the three other nanobodies we tested (Nb2, Nb3, Nb4), which did not have enrichment ratios significantly above the background (Fig. 4B). To better understand how Nb1 stabilized this interaction, we created nanoswitches that contained smaller portions of the spike protein as well as ACE2. Nb1 increased looping between ACE2 and the S1 or receptor-binding domain (RBD) regions of the spike protein (Fig. 4B and fig. S8F). Thus, the RBD portion of the spike trimer appears to be sufficient for observation of Nb1-dependent enhancement of ACE2 binding. However, other contributions from other regions in the context of the full trimer cannot be excluded.

We performed gel filtration of a 1:1:1 mixture of ACE2:RBD:Nb1 and found the formation of a stable complex containing all three proteins (Fig. 4C). Similarly, we ran blue native polyacrylamide gel electrophoresis and found a high molecular weight complex of all three proteins, whereas RBD and ACE2 alone did not form a stable, observable complex in the absence of Nb1 (fig. S8G). Pull-down experiments confirmed that adding Nb1 caused immobilized spike trimer to pull down increased ACE2 and immobilized ACE2 to pull down increased RBD (fig. S8H). We gathered dose-response curves and found that Nb1 had a low nanomolar EC_{50} for increasing the interaction between ACE2 and the spike trimer or RBD, indicating the formation of an energetically stable three-body complex (Fig. 4D). We also measured the apparent off-rate kinetics of the interaction between ACE2 and the RBD. We did this by allowing the nanoswitches to equilibrate, then adding 2 μM of RBD in solution to suppress relooping if the ACE2 and RBD on the nanoswitches dissociated from each other. We then measured the decrease in looped-band intensity at specified time points after the addition of soluble RBD and fit the looped-band intensities to an exponential decay curve (Fig. 4E). The fitted dissociation rate constant

Downloaded from https://www.science.org at Harvard University on November 05, 2026

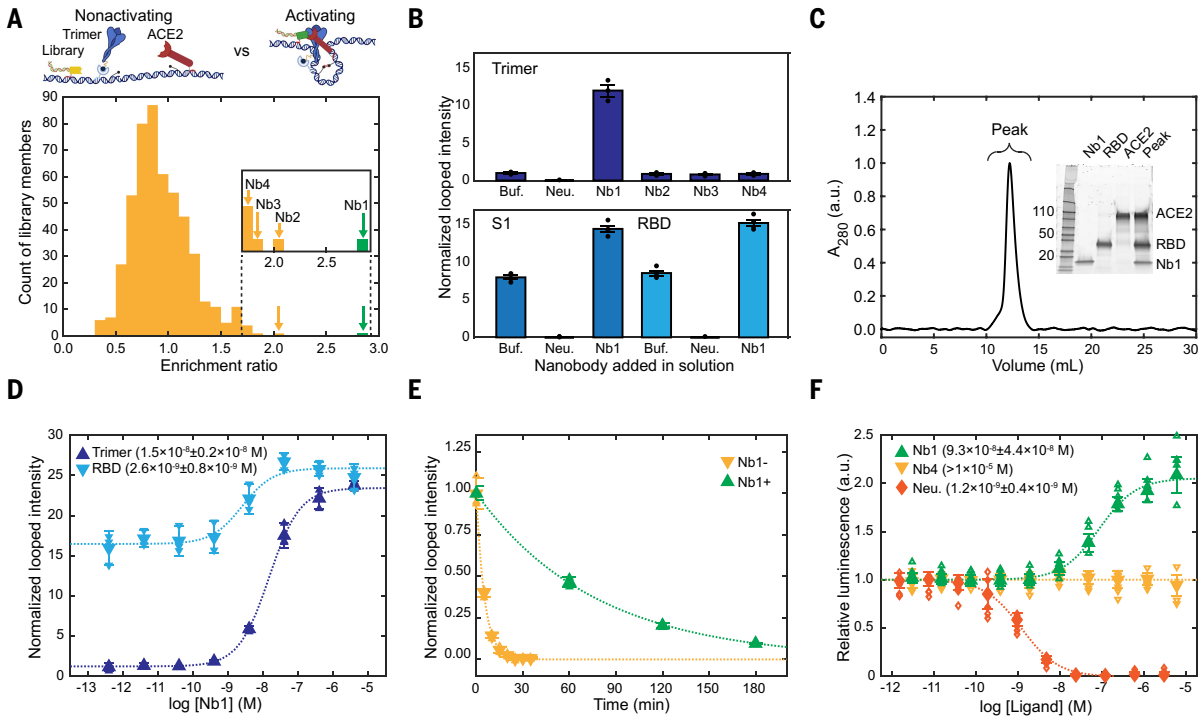


Fig. 4. Discovery of a SARS-CoV-2 protein-protein interaction enhancer. (**A**) Enrichment of the 500 most abundant nanobodies from FIND selection. Enrichment is given by the average of the proportion of counts for each nanobody in the looped fraction over three technical replicates, divided by the average of the proportion of counts for each nanobody in the unlooped fraction over the same three technical replicates. Nanobodies were labeled according to their enrichment rank, with Nb1 indicated in green with an arrow. The "barcode" that encodes the nanobody sequence is shown as the red and green mRNA-DNA hybrid attached to the orange nanobody in the schematic. [Created with BioRender.com (2026); https://BioRender.com/lynhjx2] (**B**) Nanoswitch looping between SARS-CoV-2 spike trimer (top), S1 protein (bottom left), or RBD protein (bottom right) and ACE2 in the presence of 2 μM of the indicated nanobody. For the neutralizing nanobody (Neu.), we used Clone # L009.1.32N (R&D Systems). Normalized looped intensity (I_{Loop}) represents the raw looped intensity of the signal (I_{Raw}) with the background intensity in the absence of any spike protein on the nanoswitch subtracted (I_{Zero}) and then normalized by the background-subtracted intensity of the spike-trimer nanoswitch in the absence of any nanobody ($I_{Trimer,Buf} - I_{Zero}$), in other words, $I_{Loop} = (I_{Raw} - I_{Zero})/(I_{Trimer,Buf} - I_{Zero})$ ($N = 4$, SEM). Looping was lower for the spike trimer in buffer as compared with S1 and RBD because RBDs on the spike sample closed conformations that reduce ACE2 accessibility relative to isolated S1 and RBD constructs. (**C**) Gel-filtration chromatography of a 1:1:1 mixture of NB1:RBD:ACE2. a.u., arbitrary units. (Inset) Peak fraction and Nb1, RBD, and ACE2 reference lanes on Krypton-stained SDS-PAGE. (**D**) Nanoswitch looping between SARS-CoV-2 spike trimer (dark blue triangles) or RBD protein (light blue upside-down triangles) and ACE2 in the presence of serial dilutions of Nb1 ($N = 3$, SEM). The data are fit to $A/(1 + EC_{50}/[Nb1]) + B$; EC_{50} values are presented in the legend with 95% confidence intervals. (**E**) Dissociation of ACE2 and RBD in the absence (inverted triangle) or presence (triangle) of Nb1, with superimposed fits to an exponential decay model with an offset. Looped-band intensities were fit to $I(t) = A\exp(-k_{off}\,t) + B$; for plotting data were normalized as $[I(t) - B]/A$ ($N = 4$, SEM). (**F**) ACE2-expressing HEK293 cells were challenged with pseudotyped SARS-CoV-2 lentivirus in the presence of serial dilutions of the indicated nanobody. Luminescence was measured 48 hours after infection as a readout for virus infectivity. Data are graphed as percent neutralization relative to virus-only infection control ($N = 6$ biological replicates, SEM). The data are fit to $A/(1 + EC_{50}/[Ligand]) + B$; EC_{50} values are presented in the legend with 95% confidence intervals.

(k_{off}) reports the apparent dissociation rate between ACE2 and RBD because these are the two proteins attached directly to the nanoswitch, whereas Nb1 may be present or absent as a soluble stabilizing nanobody. The off-rate decreased by a factor of ~350 in the presence of 2 μM Nb1, owing to a strong, stabilizing effect. In the absence of Nb1, the average lifetimes we measured corresponded to k_{off} values on the order of 10^{-3} to 10^{-4} s^{-1} (the average lifetime was 5.3 min for the reference variant, and 33.7 min for the Alpha variant; fig. S9), which were in reasonable agreement with published measurements of ACE2-RBD kinetics (*41*–*44*). We also studied the effect of mutations on Nb1 enhancement (supplementary text and fig. S9).

SARS-CoV-2 pseudovirus assay of enhancing nanobody Nb1

The stabilizing effect of Nb1 on the interaction between ACE2 and spike trimer indicated that Nb1 might also increase infectivity of SARS-CoV-2. To test this, we used pseudotyped SARS-CoV-2 lentivirus to quantify the effect of Nb1 on infectivity against ACE2-expressing human embryonic kidney 293 (HEK293) cells. Nb1 increased infectivity in a dose-dependent manner (Fig. 4F). In contrast, Nb4, which did not increase ACE2 binding to the spike trimer (Fig. 4B), did not increase infectivity. As a control, we also included a known neutralizing nanobody that decreased infectivity.

Affinity maturation of Nb1

To improve on initial hits, we performed FIND on a mutational library around Nb1. This library was created with up to one mutation in each of the three complementarity-determining region (CDR) sequences, resulting in ~13 million different sequences. We performed FIND on this library without any bead-based prescreening and identified nanobodies with both higher and lower predicted activity than that of Nb1 on the basis of their nanoswitch-based enrichment ratios (fig. S10A). To validate these predictions, we selected and expressed five nanobodies with higher enrichment ratios and five with lower enrichment ratios. All 10 nanobodies displayed the expected activity relative to Nb1, supporting the use of the enrichment ratio as a proxy for stabilization activity (fig. S10B).

Downloaded from https://www.science.org at Harvard University on November 05, 2026

Discovery of a PPARγ agonist

To demonstrate discovery of small-molecule modulators from a large DEL, we selected for agonists of PPARγ. PPARγ is a nuclear receptor and transcription factor that regulates lipid storage and glucose metabolism (*45*). When activated, PPARγ forms complexes with other proteins to activate the transcription of numerous genes that increase sensitivity to insulin. Therefore, small-molecule agonists that activate PPARγ have had use in treating diabetes (*45*, *46*). To screen for agonists, we created nanoswitches that contained both the ligand-binding domain of PPARγ and a peptide sequence from the CREB-binding protein (CBP-1) transcriptional coactivator. For these nanoswitches, PPARγ agonists, such as rosiglitazone, should increase PPARγ's ability to bind to CBP-1 and therefore increase looping intensity (Fig. 5A). We used a 400-million member DEL and performed one round of bead-based prescreening before nanoswitch screening. For nanoswitch-based screening, we attached PPARγ, the CBP-1 peptide, and a member of an enriched DEL to each DNA scaffold. For attachment of the DEL to the nanoswitch, we used an oligonucleotide that contained a flexible PEG18 linker in between the sequence that bound to the nanoswitch and the sequence that bound to the single-stranded end of each DEL member. We selected the two library members with the highest enrichment ratio for synthesis and further verification (Fig. 5B). Chemical structures of Ligands A and B are shown in fig. S11. FIND identified these two ligands as agonists, even though they were not the top by abundance through bead-based enrichment (fig. S12). We used an orthogonal, commercially available time-resolved Förster resonance energy transfer (TR-FRET) assay to confirm that both chosen ligands increased interaction between PPARγ and a CBP-1 peptide (Fig. 5C). We also measured the effect of our ligands in a cellular assay and both increased lipid accumulation, consistent with PPARγ activation (Fig. 5D). The two ligands are not similar in structure to rosiglitazone (Tanimoto similarity ≤ 0.31) or any other ligand in the ChEMBL database (Tanimoto similarity ≤ 0.62).

Conclusions

We introduce FIND as a tool to discover novel compounds with specific functional characteristics in an ultrahigh-throughput manner. FIND combines DNA nanoswitches with nucleotide-encoded libraries and next-generation sequencing to select for molecular modulators in an accessible, multiplexed assay. We demonstrated this capability at scales spanning ~10^8 members (small-molecule DEL) and ~10^{10} members (mRNA-display nanobody library). In our first demonstration, we identified known agonists of the GPCR β_2AR. Although other studies have found small molecules that bind to GPCRs (*47*, *48*), enrichment in these previous selection assays was generally based on binding to the receptor, rather than on detecting a functional change in the receptor upon ligand binding. Thus, follow-up functional assays were previously required to distinguish simple binders from molecular modulators.

We also demonstrated de novo discovery from a naïve library by using FIND to identify a nanobody that strongly stabilizes the interaction between the RBD of the SARS-CoV-2 spike protein and ACE2. Antibodies that cause ADE for SARS-CoV-2 can act by either Fc-receptor–mediated or Fc-receptor–independent infection enhancement (*37*, *38*). In a previous study, antibodies were discovered that bind to the N-terminal domains of two adjacent spike trimers to induce the open conformation of RBD, thus enhancing the binding capacity of spike protein to ACE2 and the infectivity of SARS-CoV-2 (*37*). The mechanism for ADE we present here is different, with the nanobody activity consistent with stabilizing the ACE2-RBD interaction, potentially through ternary complex formation, to enhance the binding between spike protein and ACE2.

Finally, we demonstrated FIND for de novo small-molecule discovery by screening a 400-million member DEL for PPARγ agonists. We identified two ligands that increased PPARγ–CBP-1 association and confirmed their activity in an orthogonal TR-FRET assay and a lipid accumulation cellular assay, consistent with PPARγ activation.

The tools introduced here are not limited to the specific examples provided. Because nanoswitch constructs are modular and compatible with nucleotide-encoded libraries spanning both small molecules and biologics, FIND has the potential to be adapted to additional interaction systems. Compared to other multiplexed interaction-profiling methods (*49*), the selection step in FIND uses standard gel electrophoresis and enables selection on the basis of interaction state rather than affinity alone. Mechanistic assignment generally requires additional biochemical characterization beyond the initial interaction outcome-based screen. Because the readout is gel electrophoresis–based, nanoswitch follow-up assays are performed in microliter-scale reactions (typically ~10 μl) and resolved by a ~100-min gel run under our conditions, providing time point multicomponent profiling that complements real-time biophysical methods such as surface plasmon resonance and biolayer interferometry. By leveraging advances in DNA nanotechnology, FIND provides a powerful and accessible research tool that should accelerate the discovery and characterization of novel therapeutics to treat diseases.

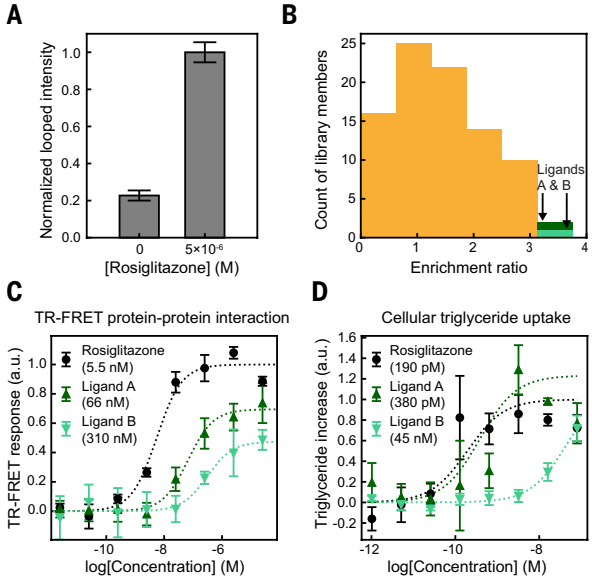


Fig. 5. Discovery of small-molecule PPARγ agonists. (**A**) Nanoswitches containing PPARγ and CBP-1 show increased loop formation in the presence of the agonist rosiglitazone ($N = 4$). (**B**) Enrichment ratios of the 90 most abundant DEL members from FIND selection. Enrichment ratio is given by the average of the proportion of counts for each library member in the looped fraction over eight technical replicates, divided by the average of the proportion of counts for each library member in the unlooped fraction over the same eight technical replicates. Ligands A and B have the highest enrichment values and are highlighted in green. Their chemical structures are shown in fig. S11. (**C**) TR-FRET assay of the interaction between PPARγ and the coactivator peptide CBP-1 in the presence of increasing concentrations of rosiglitazone, Ligand A, and Ligand B. Results are normalized to rosiglitazone. The data are fit to $A/(1 + EC_{50}/[\text{Ligand}]) + B$, with EC_{50} values as given in the legend. Error bars are SEM over $N = 3$ replicates for Ligands A and B, and $N = 4$ replicates for rosiglitazone. (**D**) Lipid accumulation of OP9 cells during adipocyte differentiation in the presence of the indicated compounds ($N = 4$, SEM). Results are normalized to the maximal rosiglitazone activity. The data are fit to $A/(1 + EC_{50}/[\text{Ligand}]) + B$, with EC_{50} values as given in the legend.

Downloaded from https://www.science.org at Harvard University on November 05, 2026

Materials and methods

Protein expression and purification

The human β_2AR gene was cloned into baculovirus transfer vector PVL1392 with modifications to add a hemagglutinin signal peptide and FLAG epitope tag to the receptor's N terminus. The receptor construct was additionally modified by introduction of a 3C protease site after Gly^{365}, allowing proteolytic removal of the receptor's unstructured distal carboxy terminus. Baculovirus was produced in Sf9 insect cells using the BestBac system (Expression Systems) according to manufacturer's instructions. For protein production, Sf9 cells were grown at 27°C with shaking at 130 rpm and were infected with baculovirus at a density of 4 million cells/ml. Alprenolol (Sigma) was added immediately after infection to a final concentration of 1 μM, and cells were incubated for 60 hours to allow receptor expression.

Cells were harvested by centrifugation at 4000*g* for 15 min. Cells from 2 liters of culture were resuspended in 300 ml of lysis buffer consisting of 20 mM HEPES pH 7.5, 2 mM magnesium chloride, 2 μl benzonase (Sigma), 1 μM alprenolol, and a complete protease inhibitor tablet (Roche). Following resuspension, cells were centrifuged at 4000*g*, and the resulting supernatant was discarded. The pellet was resuspended in 300 ml of solubilization buffer consisting of 200 mM sodium chloride, 10% (v/v) glycerol, 20 mM HEPES pH 7.5, 1% LMNG (Anatrace), 0.1% (w/v) CHS (Steraloids), and 1 μM alprenolol (Sigma). The resulting suspension was homogenized in a glass dounce tissue grinder and then stirred for two hours at 4°C, before centrifugation at 50,000*g* for 30 min. The supernatant was decanted into a beaker, and pellets were discarded. Calcium chloride was added to the solubilized membranes to a final concentration of 2 mM. Solubilized material was loaded over an anti-FLAG affinity chromatography resin followed by washing with 10 column volumes of wash buffer consisting of 0.01% (w/v) LMNG, 20 mM HEPES pH 7.5, 1 μM alprenolol, 2 mM calcium chloride, and 150 mM sodium chloride. Receptor was eluted in the same buffer without calcium chloride or alprenolol but with 0.2 mg/ml FLAG peptide (Genscript) and 5 mM EDTA added. Receptor was concentrated by centrifugal concentration and then purified by size exclusion chromatography (SEC) using a Superdex 200 10/300 column (GE Healthcare) in a buffer of 0.01% (w/v) LMNG, 20 mM HEPES pH 7.5, and 150 mM sodium chloride. Receptor was concentrated and flash frozen with 20% (v/v) glycerol for storage at −80°C before use.

Nanobodies were expressed from pET26b plasmid in *Escherichia coli* strain BL21(DE3) and were purified from periplasm by osmotic shock and nickel affinity chromatography as described previously (*40*). Purified nanobodies were dialyzed into 20 mM HEPES pH 7.5, 150 mM sodium chloride and flash frozen with 20% (v/v) glycerol at −80°C before use.

$MiniG_S$ construct 414 was cloned with an N-terminal His-tag and 3C protease cleavage site into pET28a (*35*). An additional mutation of a surface-exposed cysteine residue (C82S) was introduced to prevent disulfide bond–mediated interactions during FIND assays. The C82S $miniG_S$ protein was expressed in *E. coli* strain BL21 (DE3) after induction with 1 mM isopropyl-β-D-thiogalactopyranoside (IPTG) for 18 hours at 20°C and purified with a protocol based on the previously reported method (*35*). Cells were harvested by centrifugation at 4000*g* for 30 min at 4°C and lysed by sonication in a buffer comprising 40 mM HEPES pH 7.5, 100 mM NaCl, 10% glycerol, 10 mM imidazole, 5 mM $MgCl_2$, 50 μM guanosine diphosphate (GDP), 1 mM phenylmethylsulfonyl fluoride, 1:100,000 (v:v) benzonase, 100 μM dithiothreitol (DTT), and protease inhibitor tablets (Roche). The lysate was centrifuged at 50,000*g* for 30 min at 4°C, and the supernatant was filtered with glass microfiber filters (VWR). Filtered supernatant was loaded onto 10 ml HisPur cobalt resin (Thermo Scientific); washed with 20 mM HEPES pH 7.5, 500 mM NaCl, 10 mM imidazole, 10% glycerol, 1 mM $MgCl_2$, and 50 μM GDP; then eluted with 20 mM HEPES pH 7.5, 100 mM NaCl, 250 mM imidazole, 10% glycerol, 1 mM $MgCl_2$, and 50 μM GDP. 3C protease was added to the eluted protein, and the sample was dialyzed overnight in 20 mM HEPES pH 7.5, 100 mM NaCl, 10% glycerol, 1 mM $MgCl_2$, and 10 μM GDP. After dialysis, the sample was loaded onto 5 ml HisPur cobalt resin (Thermo Scientific) to remove the 3C protease by negative purification. The sample was concentrated and loaded onto a Sephadex S200 column (GE Healthcare) equilibrated with 10 mM HEPES pH 7.5, 100 mM NaCl, 10% glycerol, 1 mM $MgCl_2$, 1 μM GDP, and 100 μM tris(2-carboxyethyl)phosphine hydrochloride. Peak fractions were concentrated, then aliquots were flash frozen in liquid nitrogen and stored at −80°C.

For nanobodies we found against the spike-trimer, sequences containing C-terminal glycine-serine linker, poly-lysine labeling site, and hexa-histidine tag were synthesized as a gene block (Integrated DNA Technologies). Polymerase chain reaction (PCR) primers NbEXP_Freal and NbExp_R_Lys were used to amplify the sequence and add the 5′ NcoI and 3′ XhoI restriction sites. We then ligated the sequences into pET-26b(+) (Novagen) using T4 DNA Ligase (Invitrogen) and transformed into BL21(DE3) competent *E. coli* (NEB) according to the manufacturer's protocol. Positive colonies on kanamycin plates were picked and sequenced, and confirmed colonies were subcultured overnight at 37°C in 10 ml in LB-kanamycin broth shaking at 200 rpm. Ten milliliters of subculture was added to 500 ml of LB-kanamycin and grown out for 2 hours at 37°C shaking at 200 rpm. To induce periplasmic nanobody expression, IPTG was added to the culture at 1 mM final concentration and incubated at 25°C overnight with shaking at 200 rpm. The cells were harvested and pelleted at 3500*g* for 10 min. Tris-EDTA-sucrose (TES) buffer (200 mM Tris-HCl pH 7.5/1 mM EDTA/0.5 M sucrose; volume: 12.5 ml) was added to resolubilize the pellet and incubated at room temperature (RT) for 45 min. To induce osmolysis, 25 ml of double distilled water (ddH_2O) was added, rapidly mixed, and incubated at RT for 45 min. To isolate the periplasmic fraction, the lysate was ultracentrifuged at 20,000*g* at 4°C for 20 min. To quench the EDTA and equilibrate the periplasmic isolate for Ni-NTA purification (Ni-NTA High Performance Sepharose, Cytiva), quenching buffer was added to bring the solution to final concentrations of 20 mM $MgCl_2$, 300 mM NaCl, 75 mM imidazole, and 0.05% Tween-20. Nanobodies were eluted in EDTA and desalted with 7K MWCO Zeba desalting columns (Thermo Scientific) to phosphate-buffered saline (PBS). For nanoswitch assays, Ni-NTA purified nanobodies were used. For cellular assays, Ni-NTA nanobodies were further purified by SEC on a Superdex S75 10/300GL (Cytiva).

The ligand binding domain of PPARγ with an N-terminal avi-tag peptide sequence was expressed in Sf9 cells, purified by anion exchange with a Q column, purified by SEC with a Chromdex 75, biotinylated in vitro, and then concentrated in 50 mM Tris-HCl, 150 mM NaCl, 5% glycerol, 0.3 mM DTT, pH 8.0. The CBP-1 peptide {Pra} GGSGGNLVPDAASKHKQLSELLRGGSGS was synthesized with a propargylglycine at the N terminus for attachment to an oligonucleotide through click-chemistry (Genscript).

Protein coupling

β_2AR, nanobodies, monomeric streptavidin (Sigma), and ACE2 (Acrobiosystems) were coupled to azide-modified oligonucleotides (Integrated DNA technologies). Specifically, for β_2AR we attached VarD_azide_3 at the single exposed cysteine (Cys^{265}) using a DBCO-PEG4-Maleimide linker (Sigma) in 10 mM HEPES pH 7.5, 50 mM NaCl, 0.01% LMNG, and 0.001% CHS. A 10-fold molar excess of linker and 20-fold molar excess of oligonucleotide were used. The receptor was then purified using ANTI-FLAG M2 Magnetic Beads (Sigma) and eluted with FLAG-peptide (Sigma). For Nb60 and Nb80, we attached Var7_azide_5 nonspecifically to a surface lysine using a DBCO-PEG4-NHS ester linker (Sigma) in 50 mM HEPES pH 8.6 and 50 mM NaCl. We used an equimolar amount of linker and 5× excess of oligonucleotide. We then purified the nanobodies using Ni Sepharose High Performance (GE). We similarly coupled monomeric streptavidin to VarD_azide_3 and ACE2 to Var7_azide_5 and purified using Ni

Downloaded from https://www.science.org at Harvard University on November 05, 2026

Sepharose High Performance (GE). Starting protein concentrations were 50, 80, and 13 μM for β_2AR, monomeric streptavidin, and ACE2, respectively. For attachment of the CBP-1 peptide to an oligonucleotide, we followed the procedure of Koussa *et al.* (*14*). Coupled protein concentrations were measured against a known reference DNA concentration on a 4–20% tris-borate EDTA (TBE) gel stained with SYBR Gold. The resulting coupled proteins will mostly have one or no oligonucleotides attached. Overcoupling too many oligonucleotides to proteins could interfere with binding.

Nanoswitch formation

DNA nanoswitches were created as previously described (*14*). Briefly, circular single-stranded DNA (ssDNA) from the 7249-nt bacteriophage M13 (New England BioLabs) was linearized by enzymatic cleavage of a single site using BtscI (New England BioLabs) and a site-specific oligonucleotide. This ssDNA scaffold was mixed with a molar excess of tiling 60-mer oligonucleotides (10:1), excluding the complementary regions for latch and other specific components to hybridize. For the stem-loop nanoswitches, we included 10× stem-loop, 10× complementary oligonucleotide, and, if needed, 4× capture oligonucleotide and 10× library, in 10 mM HEPES pH 7.5, 50 mM NaCl, 10 mM $MgCl_2$. For β_2AR nanoswitches, we included 4× receptor, 10× nanobody, and, if needed, 4× capture oligonucleotide and 10× DNA-encoded compounds in 10 mM HEPES pH 7.5, 50 mM NaCl, 10 mM $MgCl_2$, 0.01% LMNG, and 0.001% CHS. For the latch, we used 8× TCO-modified latch oligonucleotides VarDlatch_TCO_3 and Var7latch_TCO_5. We similarly created nanoswitches for the spike-trimer/ACE2 mRNA display screen, including 6× monomeric streptavidin and 6× ACE2 Nanoswitches for the PPARγ/CBP-1 DEL screen were prepared by including 6× monomeric streptavidin and 6× CBP-1 peptide.

Incubation and gel electrophoresis

For each 10-μl sample, we mixed together nanoswitch at 130 pM and ligand in 10 mM HEPES pH 7.5, 50 mM NaCl, 10 mM $MgCl_2$, 0.01% LMNG, and 0.001% CHS and incubated for 2 hours. For competition experiments, we incubated for 6 hours. After incubation, 9 μl of sample was added to 1.8 μl of 7.5 μM tetrazine-PEG5-tetrazine (Conju-Probe). The concentration of tetrazine linker was chosen to maximize the difference in signal between agonist and antagonist (fig. S2A). Given the rapid nature of the TCO-tetrazine reaction, the latch reaction takes only tens of seconds to complete (fig. S2, B and C). Blue/orange loading dye (Promega) was added, and samples were resolved on a prestained SYBR gold 0.7% ultrapure agarose gel (Thermo Fisher) for 100 min at 100 V. Gels were imaged using a laser gel-scanner (GE Typhoon). Looped intensity was quantified by integrating the area under the curve after median filtering and linear background subtraction (*14*). All experiments were normalized to the looped intensities in the presence and absence of BI167107. For saturating amounts of ligand, we used a concentration of 4×10^{-4} M.

Stem-loop enrichment

For individual attached library member experiments, we incubated the samples for 1 hour in 10 mM HEPES pH 7.5, 50 mM NaCl, and 10 mM $MgCl_2$ and quantified looped intensity on an agarose gel. We also included a latch to stabilize the loop. All intensities were normalized to the intensity of fully on stem-loops in the presence of 1×10^{-5} M loop_open (table S2). For the multiplexed experiments, the bands of interest were cut out using a Safe Imager 2.0 Blue Light Transilluminator light. Because the looped band was not visible, the corresponding gel region was cut out on the basis of the position of reference samples with the same loop size that were also run on the gel. DNA from the extracted agarose was electroeluted into 0.5× TBE using 8 kDa MWCO MINI GeBaFlex-tubes. Samples were then prepared for sequencing by ligating on one of four sequences: Ligation_1, Ligation_2, Ligation_3, or Ligation_4 (table S2). Each of these sequences has a specific barcode so each sequencing lane can read four pooled samples. The ligations were performed by mixing the eluted DNA with 5×10^{-10} M splint and 1×10^{-9} M ligation in T4 DNA ligase buffer, performing a temperature ramp from 90°C to 25°C, adding T4 DNA ligase, incubating for 2 hours, and then heat inactivating at 65°C for 10 min. Samples were then prepared for sequencing with PCR using Q5 polymerase and primers Seq_F and Seq_R. Then we ran the products on a 10% TBE polyacrylamide gel and cut out the amplified band, which was then broken up by spinning in a gel breaker tube (Ist Engineering) and eluted overnight in 10 mM Tris, pH 7.5. Then we purified the products by running them through a 0.45 μm Spin-X Centrifuge Tube Filter (Corning) and ethanol precipitating. The sequencing was multiplexed on a MiSeq with 3.7 to 6.9 million reads per extracted band.

Stem-loop sequencing analysis

All reads were first mapped to one of four 7mer indices, allowing for up to two mismatches. Then the counts for each of the sequences corresponding to each library member were added up for each sample. The enrichment was then calculated as the ratio of the number of reads in the looped sample over the number of reads in the unlooped sample, normalized by the ratio of the total number of counts in each sample. For the stem-loop enrichment data, we filtered out sequences that had an average enrichment of >1.5 over two experiments, in which we omitted the stem-loop. This filtered out 235 sequences out of 4096 total. All analysis was performed using custom MATLAB scripts.

Synthesis of TS218

The β_2AR agonist TS218 was synthesized following the synthetic route depicted in fig. S5, with nuclear magnetic resonance (NMR) spectra in figs. S13 to S17. Reagents and dry solvents were of commercial quality and were used as purchased. Mass spectrometry was run on a BRUKER ESQUIRE 2000 by electrospray ionization (ESI). High-resolution mass spectrometry ESI (HRMS-ESI) was run on an AB Sciex Triple TOF660 SCiex, source type ESI. NMR spectra were obtained on a Bruker Avance 400 (400 MHz for ^{1}H and 101 MHz for ^{13}C) or a Bruker Avance 600 spectrometer (600 MHz for ^{1}H and 151 MHz for ^{13}C) at 300 K using the solvents indicated. The chemical shifts were reported in parts per million (δ) relative to tetramethylsilane. Purification by flash column chromatography was performed using silica gel 60. Thin-layer chromatography analyses were performed on Merck 60 F254 aluminum sheets and visualized by UV detection (254 nm). High-performance liquid chromatography (HPLC) analysis was conducted on an Agilent 1200 HPLC system using a DAD detector and with a ZORBAX ECLIPSE XDB-C8 (4.6 mm by 150 mm, 5 μm) column using the following solvent system: CH_3CN/0.1% aq. TFA, 10% CH_3CN for 3 min, to 95% in 15 min, 100% for 6 min, to 10% in 3 min, 10% for 3 min, flow rate 0.5 ml/min. Preparative HPLC was performed on an Agilent 1100 Preparative Series, using a *ZORBAX ECLIPSE XDB-C8 PrepHT* column (21.5 mm by 150 mm, 5 μm, flow rate 10 ml/min) with the solvent systems indicated and a detection wavelength of 230 nm.

Compound **2**, *tert*-butyl (6-hydroxyhexyl)carbamate, was prepared following a literature protocol (*50*). 6-Aminohexan-1-ol (**1**) (1.00 g, 8.53 mmol) and di-*tert*-butyldicarbonate (1.86 g, 8.53 mmol) were dissolved in 5.0 ml anhydrous tetrahydrofuran (THF) and stirred at RT for 3 hours. The solvent was evaporated using a rotavapor and the colorless oil was dried in vacuo to obtain **2** (1.84 g, 99%) as a colorless wax. ^{1}H-NMR (400 MHz, $CDCl_3$) δ (ppm) 1.29–1.42 (m, 4H), 1.44 (s, 9H), 1.46–1.62 (m, 4H), 1.72 (s, 1H), 3.12 (dt, J = 6.5, 6.5 Hz, 2H), 3.64 (t, J = 6.5 Hz, 2H), 4.54 (s, 1H). ^{13}C NMR (151 MHz, $CDCl_3$) δ (ppm) 25.4, 26.5, 28.6, 30.2, 32.7, 40.5, 62.8, 80.9, 156.2. ESI-MS m/z 240.0 $[M+Na]^+$.

Compound ***3***, 6-((*tert*-butoxycarbonyl)amino)hexyl methanesulfonate, was prepared following a literature protocol (*51*). Compound **2** (1.8 g, 8.5 mmol) and triethylamine (1.2 ml, 8.5 mmol) were dissolved in 10 ml THF and cooled to 0°C in an ice bath. Methanesulfonyl

Downloaded from https://www.science.org at Harvard University on November 05, 2026

chloride (0.66 ml, 8.5 mmol) was added dropwise, and the reaction was stirred for 2 hours at RT. The solvent was evaporated, the residue was taken up in dichloromethane and water, and the aqueous layer were extracted with dichloromethane. The combined organic layers were washed with water and brine and dried over Na_2SO_4. The solvent was evaporated, and the crude product was used in the next step without further purification (2.4 g, 97%). ^{1}H-NMR (600 MHz, $CDCl_3$) δ (ppm) 1.32–1.38 (m, 2H), 1.39–1.45 (m, 2H), 1.44 (s, 9H), 1.46–1.53 (m, 2H), 1.63 (s, 1H), 1.72–1.78 (m, 2H), 3.00 (s, 3H), 3.11 (dt, J = 6.5, 6.5 Hz, 2H), 4.22 (t, J = 6.5 Hz, 2H), 4.53 (s, 1H). ^{13}C NMR (101 MHz, $CDCl_3$) δ (ppm) 25.3, 26.3, 28.6, 29.2, 30.1, 37.5, 40.5, 70.0, 79.3, 156.1. ESI-MS m/z 318.1 $[M+Na]^+$.

Compound **4**, *tert*-butyl-(6-(4-(2-hydroxyethyl)-2-methoxyphenoxy) hexyl)carbamate, was prepared by suspending homovanillyl alcohol (0.25 g, 1.5 mmol), **3** (0.48 g, 1.6 mmol), potassium carbonate (0.41 g, 3.0 mmol), and potassium-iodide (49 mg, 0.30 mmol) in 5.0 ml acetonitrile and heated to reflux for 16 hours. The solvent was evaporated, and the residue was mixed with water, extracted with dichloromethane, washed with brine, and dried over Na_2SO_4. The solvent was evaporated and the crude product was purified via flash column chromatography on silica gel (eluent: n-hexane/ethyl acetate = 2/1 to 1/1) to give compound **4** (0.48 g, 88%). ^{1}H-NMR (600 MHz, $CDCl_3$) δ (ppm) 1.34–1.42 (m, 2H), 1.44 (s, 9H), 1.45–1.53 (m, 4H), 1.79–1.87 (m, 2H), 2.81 (t, J = 6.4 Hz, 2H), 3.12 (dt, J = 6.5, 6.5 Hz, 2H), 3.84 (t, J = 6.5 Hz, 2H), 3.86 (s, 3H), 3.99 (t, J = 6.7 Hz, 2H), 4.52 (s, 1H), 6.72–6.77 (m, 2H), 6.79–6.84 (m, 1H). ^{13}C NMR (151 MHz, $CDCl_3$) δ (ppm) 25.9, 26.7, 28.6, 29.3, 30.1, 38.9, 40.7, 56.1, 63.9, 69.2, 79.2, 112.9, 113.5, 121.1, 131.2, 147.4, 149.7, 156.2. ESI-MS m/z 390.2 $[M+Na]^+$. HPLC (254 nm): t_R = 17.8 min, purity: 98%.

Compound **5**, 4-((6-((*tert*-butoxycarbonyl)amino)hexyl)oxy)-3-methoxyphenethyl methanesulfonate, was prepared by dissolving compound **4** (0.30 g, 0.82 mmol) in 5.0 ml anhydrous dichloromethane and triethylamine (0.13 ml, 0.90 mmol) and cooled to 0°C in an ice bath. Subsequently, methanesulfonyl chloride (70 µl, 0.90 mmol) was added, and the solution was stirred for 90 min at RT. Water was added, and the reaction mixture was extracted with dichloromethane, washed with brine, and dried over Na_2SO_4. The solvent was evaporated, and the crude product was purified via flash column chromatography on silica gel (eluent: n-hexane/ethyl acetate = 1/1) to obtain compound **5** (0.33 g, 90%). ^{1}H-NMR (600 MHz, $CDCl_3$) δ (ppm) 1.35–1.41 (m, 2H), 1.44 (s, 9H), 1.45–1.54 (m, 4H), 1.78–1.86 (m, 2H), 2.87 (s, 3H), 2.99 (t, J = 7.0 Hz, 2H), 3.12 (dt, J = 6.5, 6.5 Hz, 2H), 3.86 (s, 3H), 3.98 (t, J = 6.7 Hz, 2H), 4.39 (t, J = 7.0 Hz, 2H), 4.51 (s, 1H), 6.74–6.76 (m, 2H), 6.80–6.83 (m, 1H). ^{13}C NMR (151 MHz, $CDCl_3$) δ (ppm) 25.9, 26.7, 28.6, 29.3, 30.2, 35.4, 37.6, 40.7, 56.2, 69.1, 70.6, 112.9, 113.4, 121.2, 128.9, 147.8, 149.7, 156.1. ESI-MS m/z 468.2 $[M+Na]^+$. HPLC (254 nm): t_R = 18.9 min, purity: 95%.

TS218 ((*R*)-4-(2-((4-((6-aminohexyl)oxy)-3-methoxyphenethyl) amino)-1-hydroxyethyl)benzene-1,2-diol trifluoracetate) was prepared by dissolving compound **5** (0.10 g, 0.22 mmol) and (*R*)-noradrenaline (0.11 g, 0.67 mmol) in 2.0 ml of anhydrous dimethyl sulfoxide (DMSO) under argon atmosphere and heated to 70°C while stirring for 16 hours. The solution was diluted with water and lyophilized. The residue was taken up in 1.0 ml dichloromethane/TFA (2/1) and stirred under argon gas atmosphere for 16 hours at RT. The solvent was removed using a rotavapor, and the residue was purified via preparative HPLC (RP-C8, CH_3CN/0.1% aq. TFA, 5-40% in 23 min) to obtain the TFA salt of compound **TS218** (5.0 mg, 3%). ^{1}H-NMR (600 MHz, DMSO-d_6) δ (ppm) 1.32–1.44 (m, 4H), 1.50–1.59 (m, 2H), 1.65–1.73 (m, 2H), 2.75–2.81 (m, 2H), 2.82–2.92 (m, 2H), 2.93–3.01 (m, 1H), 3.04–3.10 (m, 1H), 3.12–3.19 (m, 2H), 3.75 (s, 3H), 3.91 (t, J = 6.5 Hz, 2H), 4.72 (dd, J = 10.4, 3.0 Hz, 1H), 5.99 (s, 1H), 6.62 (dd, J = 8.1, 2.1 Hz, 1H), 6.70–6.75 (m, 2H), 6.88 (d, J = 8.3 Hz, 1H), 7.77 (s, 3H), 8.61 (s, 1H), 8.76 (s, 1H), 8.96 (s, 2H). ^{13}C NMR (151 MHz, DMSO-d_6) δ (ppm) 25.5, 25.9, 27.3, 29.0, 31.4, 39.2, 48.6, 53.9, 55.9, 68.5, 68.6, 113.2, 113.8, 113.8, 115.8, 117.1, 121.0, 130.1, 133.0, 145.4, 145.7, 147.4, 149.5. HRMS m/z $[M+H]^+$ calcd. 419.254049, found: 419.252889. HPLC (230 nm): t_R = 11.0 min, purity: >99%; $[\alpha]^{24}_D$ = −11.2° (0.041 in CH_3OH).

Small-molecule coupling (TS218 and BRL37344)

TS218 was coupled to an oligonucleotide through the terminal primary amine. Specifically, we mixed together azide-modified oligonucleotide at 50 µM, 3 equivalents of DBCO-PEG4-NHS ester linker (Sigma), and 15 equivalents of TS218, and incubated for 1 hour in 100 mM HEPES pH 8.5 Buffer. Excess ligand was removed with a 7K Zeba Spin Desalting Column (Thermo Fisher). Coupling was confirmed on a 20% TBE polyacrylamide gel with SYBR gold staining with a yield of >95%. BRL37344 (Sigma) was coupled to an oligonucleotide via the carboxyl group. BRL37344 (1.25 mM) was mixed with 0.0125 mM amine modified oligo, and 20 mM EDC in 100 mM MES pH 6.0 for 1 hour. Removal of excess ligand and confirmation of coupling/determination of yield was performed identically as above.

β_2AR multiplexed enrichment

Nanoswitches with attached β_2AR, Nb80, and capture oligonucleotide and DNA-encoded compounds were incubated for 1 hour in 10 mM HEPES pH 7.5, 100 mM NaCl, 10 mM $MgCl_2$, latched, and then run on a 1.0% agarose gel prestained with SYBR gold. The bands of interest were then cut out using a Safe Imager 2.0 Blue Light Transilluminator light. Because the looped band was not visible, it was cut out on the basis of the position of reference samples with the same loop size that were also run on the gel. DNA from the extracted agarose was electro-eluted into 0.5× TBE using 8 kDa MWCO MINI GeBaFlex-tubes. Samples were then prepared for sequencing with PCR using Q5 polymerase. We included custom indexing sequences for four different samples per sequencing lane, so for primers we paired Seq_R with Seq_F_1, Seq_F_2, Seq_F_3, or Seq_F_4 (table S2). After PCR, we ran the products on a 10% TBE polyacrylamide gel and cut out the amplified band, which was then broken up by spinning in a gel breaker tube (Ist Engineering) and eluted overnight in 10 mM Tris 7.5. Then we purified the products by running them through a 0.45 µm Spin-X Centrifuge Tube Filter (Corning) and ethanol precipitating. We performed the experiment in duplicate, pooled the four samples, and ran on a MiSeq with 20 million to 30 million reads.

Two-state receptor model and fitting

Looped intensities for both Nb60 and Nb80 for multiple ligands were simultaneously fit to the simple two-state model

$$A_n(L) = B_n \frac{K_n^{\text{off}} + K_n^{\text{on}} J(L)}{1 + J(L) + K_n^{\text{off}} + K_n^{\text{on}} J(L)} + C_n$$

In this equation, n = 60 or 80 for Nb60 or Nb80, K_n^{off} and K_n^{on} are the dissociation constants for the receptor to either Nb60 or Nb80 in the off and on states, and $J(L)$ is the dissociation constant for the receptor switching into the on state from the off state. We assume $J(L)$ is dependent solely on the ligand and is the same for all nanobodies. For each nanobody, C_n is the fitted offset and B_n is the fitted multiplicative constant. To find the best fit, we minimized the least squares over the eight fit parameters (four for each nanobody), weighted by the SEM of each data point for all 12 ligands for both antibodies. The $J(L)$ are additionally chosen to minimize the least squares. The fit parameters obtained with 95% confidence intervals were: $K_{60}^{\text{off}} = 3.0(2.0, 4.4)$, $K_{80}^{\text{off}} = 1.5 \times 10^{-8}\left(8.2\times10^{-9}, 2.7\times10^{-8}\right)$, $K_{60}^{\text{on}} = 0.47(0.20, 0.65)$, $K_{80}^{\text{on}} = 0.40(0.32, 0.51)$, $B_{60} = 1.5(1.4, 1.7)$, $B_{80} = 3.9(3.3, 4.9)$, $C_{60} = -0.13$ $(-0.18, -0.04)$, and $C_{80} = -0.05(-0.19, -0.02)$. We constrained the offset parameters C_{60} and C_{80} to be between −0.20 and 0.20. The confidence intervals were obtained by fits of 10,000 datasets created by Monte Carlo sampling around the actual measured values using the measured error.

Downloaded from https://www.science.org at Harvard University on November 05, 2026

Radioligand competition assay model and fitting

To test the effect of incubation time on a competitive radioligand binding assay, we modeled the full kinetic time course (fig. S7). In our model, we include a cooperativity constant, α, for each bound ligand. Consistent with our measurements, the cooperativity constant modulates the binding kinetics of nanobody-receptor binding but not the unbinding rate. Additionally, we made the cooperativity constant change the unbinding rate of the ligand when the receptor is concurrently bound to the nanobody, as addition of nanobody does not increase rate of ligand binding (*52*). We chose specific time constants and concentrations consistent with experiment. Specifically, for the agonist of interest, we used $\alpha_{60,L1} = 0.0032$, $\alpha_{80,L1} = 320$, $k_{on,L1} = 2.8 \times 10^6\ s^{-1}\ M^{-1}$, $k_{off,L1} = 0.0017\ s^{-1}$ for slow unbinding, and $k_{off,L1} = 0.17\ s^{-1}$ for fast unbinding. For the radioligand, consistent with cyanopindolol, we used $\alpha_{60,L2} = 1.1$, $\alpha_{80,L2} = 2.5$, $k_{on,L2} = 2.8 \times 10^6\ s^{-1}\ M^{-1}$, and $k_{off,L2} = 0.0017\ s^{-1}$. Additionally, for Nb80 binding to the receptor, derived from our measured off-rates and the previously measured dissociation constants (*24*), we used $k_{on,80} = 510\ s^{-1}\ M^{-1}$ and $k_{off,80} = 0.0017\ s^{-1}$, and for Nb60 we used $k_{on,60} = 3.3 \times 10^4\ s^{-1}\ M^{-1}$ and $k_{off,60} = 5.8 \times 10^{-4}\ s^{-1}$. For concentrations, we used $[Nb] = 1 \times 10^{-6}$ M, $[\beta_2AR] = 1 \times 10^{-11}$ M, and $[L2] = 6 \times 10^{-11}$ M. Starting with everything unbound, for a concentration curve of [L1], we analyzed the time course using MATLAB's ordinary differential equation solver ode45 for varying amounts of time ranging from 1.5 to 150 hours. We then extracted the inferred cooperativity parameters by fitting the end point free radioligand concentrations curves to the nonlinear system of equations that yield the concentration of free species at equilibrium (*24*), specifically

$$[R]_f = [R]_t \cdot \left\{1 + K_d[N]_f + K_1[L_1]_f\left(1+\alpha_1 K_d[N]_f\right) + K_2[L_2]_f\left(1+\alpha_2 K_d[N]_f\right)\right\}^{-1}$$

$$[N]_f = [N]_t \cdot \left\{1 + K_d[R]_f\left(1+\alpha_1 K_1[L_1]_f + \alpha_2 K_2[L_2]_f\right)\right\}^{-1}$$

$$[L_1]_f = [L_1]_t \cdot \left\{1 + K_1[R]_f\left(1+\alpha_1 K_d[N]_f\right)\right\}^{-1}$$

$$[L_2]_f = [L_2]_t \cdot \left\{1 + K_2[R]_f\left(1+\alpha_2 K_d[N]_f\right)\right\}^{-1}$$

where K_d is the dissociation constant between the receptor and nanobody, and K_i are the dissociation constants between the receptors and ligands. Here, all the binding constants are taken as known in the fitting.

Kinetic experiments

For off-rate experiments, for each 10-μl sample, we first mixed together nanoswitch at 130 pM and ligand in 10 mM HEPES pH 7.5, 50 mM NaCl, 10 mM $MgCl_2$, 0.01% LMNG, and 0.001% CHS and incubated for 2 hours. Then we added 5 μM of free nanobody to quench loop closing and latched the samples at specific time points. The normalized time-course data was then fit to an exponential decay model with an offset, $A = Be^{-k_{off}t} + C$. For the Nb80 on-rate experiments, we added a saturating amount of ligand (400 μM), and latched the samples at specific time points. The normalized time-course data were then fit to a bimolecular on-rate model with an offset, $A = B\left(1 - e^{-k'_{on}t}\right) + C$, with $k'_{on} = k_{on} + k_{off}$ the effective on-rate.

Nanobody mRNA display library construction

The core nanobody cDNA sequences, including framework and variable regions, were constructed by overlap extension PCR and purified as previously described (*40*) for each of the three loop length variant CDR3 sequences (CDR3A, CDR3B, and CDR3C). To adapt the library for mRNA display, two additional steps of overlap extension PCR and purification were used to add necessary sequences for in vitro transcription/translation and purification. First, starting cDNAs were amplified with Kruse_N_FLAG_70 and Kruse_C2HIS_LYS_1_70_short by Q5 DNA Polymerase (New England Biolabs) and gel purified. Second, gel-extracted cDNAs were amplified with N0_medium and C2HIS_LYS_2 primers by Q5 Polymerase and purified with SPRIselect (Beckman Coulter).

Generation of displayed-nanobody libraries

The mRNA display protocol for nanobodies was adapted from an established protocol (*21*). The nanobody mRNA-display cDNA library was transcribed to mRNA using the Megascript T7 in-Vitro Transcription Kit (Invitrogen). Remaining cDNA was digested by DNAseI (Invitrogen), and the mRNA was purified by Megaclear columns (Invitrogen). Then the mRNA library was ligated to a puromycin-labeled DNA linker using T4 RNA Ligase I (New England Biolabs, NEB). Excess oligo and unligated mRNA was removed first by Megaclear (Invitrogen) and then by oligo-dT pulldown (Magnetic mRNA Isolation kit, NEB). Puromycin-ligated mRNA was translated in vitro by PURExpress In Vitro Protein Synthesis Kit (NEB) according to manufacturer's protocol and stopped on ice. Next, $MgCl_2$ was added to 62.5 mM and KCl was added to 62.5 mM, and the reaction was incubated at RT for 30 min and then incubated overnight at −20°C and purified by Oligo-dT purification (NEB). Reverse Transcription of the mRNA was next performed using the Superscript III First-Strand Synthesis System (Invitrogen) with either Rtprimer_nosub (for solution panning mRNA-display) or Rtprimer_VarD (for attachment to DNA nanoswitches). Finally, the reaction mixture was purified with Ni-NTA Sepharose beads (Cytiva) and desalted with 7K MWCO Zeba desalting columns (Thermo Scientific).

Biotin solution–panning nanobody mRNA display prescreening

Solution panning for selection of nanobody libraries was performed with streptavidin T1 Dynabeads (Invitrogen). Beads were washed three times in 50 mM Tris-HCl pH 7.5, 150 mM NaCl, 0.5% bovine serum albumin (BSA), incubated for 30 min at 4°C, and then washed three times in 50 mM Tris-HCl pH 7.5, 150 mM NaCl, 0.5% BSA, 0.05% Tween-20. For the selection, we used final concentrations of 50 nM biotinylated reference SARS-CoV-2 spike trimer (Acrobiosystems) and 400 nM Human ACE2 (Sino Biological) in a buffer of 50 mM Tris-HCl pH 7.5, 150 mM NaCl, 0.5% BSA, 0.05% Tween-20, along with the displayed library. The panning reaction was incubated on ice for 10 min and then at RT for 20 min. After pulldown, the sample was eluted at 72°C for 5 min. To prepare the selected fraction for the next cycle of panning, the sample was amplified using Q5 polymerase (NEB) with C_2HIS_49bp and N_0_52bp primers and purified by SPRI (Beckman Coulter). We performed six rounds of prescreening.

Nanoswitch display screening for SARS-CoV-2 S trimer/ACE2 enhancer nanobodies

Nanoswitches with attached monomeric streptavidin and ACE2 were incubated overnight with the displayed library created with the Rtprimer_VarD RT primer in buffer with 0.5% BSA and 10 mM $MgCl_2$. The next day, EDTA was added to 50 mM and biotinylated spike-trimer (Acrobiosystems) was added to 2× excess, and incubated for 30 min. We then performed gel electrophoresis and extracted the bands as described above.

Biotin-streptavidin coprecipitation pulldown experiments

Bait and prey pairs of biotinylated SARS-CoV-2 S Trimer (Acro Biosystems) with Alexa Fluor 488 labeled (Alexa-Fluor 488 NHS ester, Invitrogen) ACE2 (Sino Biological) and biotinylated ACE2 (Sino Biological) with Alexa fluor 647 labeled (Alexa-Fluor 647 NHS ester, Invitrogen) SARS-CoV-2 Receptor Binding Domain (Sino Biological) were combined in the presence or absence of Nb1 to test for enhancement of binding. Proteins were combined in PBS, 0.05% Tween 20, 1 mg/ml BSA, with or without 1 μM of Nb1 and incubated at RT for 30 min. Streptavidin T1 Dynabeads (Invitrogen) were washed and incubated in the same buffer at RT for 30 min. Samples were added to the beads and incubated on rotation at RT for 10 min. Beads were then washed three times in buffer with 500 nM unlabeled, untagged SARS-CoV-2 RBD (Sino Biological) to prevent rebinding of labeled protein, with or without 1 μM Nb1 on rotation at room temperature for 10 min each. The sample was then eluted at 72°C for 5 min in 1x Laemmli SDS buffer

Downloaded from https://www.science.org at Harvard University on November 05, 2026

and run on a 4–20% SDS-PAGE (polyacrylamide gel electrophoresis) gel (Bio-Rad). For the second bait and prey pair of biotinylated ACE2 and 647-RBD, all experimental conditions and buffers were identical except for the starting concentrations at 100 nM (biotin-ACE2), 125 nM (647-RBD), 50 nM (biotin-Spike-Trimer), and 62.5 nM (488-ACE2), respectively.

Blue native PAGE gel-shift assay

All combinations of Nb1, RBD, and ACE2 were mixed at equimolar ratios of 1.5 μM in 15 μl and allowed to equilibrate at RT for 30 min. Samples were stained, loaded, run, and imaged on NativePAGE Novex 4–16% Bis-Tris Gels (Thermo Fisher) according to the provided manufacturer's protocol.

SEC of ACE2:RBD:Nb1 Complex

ACE2, RBD, and Nb1 proteins were mixed at equimolar ratios of 2.9 μM in 100 μl diluted in 1× PBS buffer and allowed to equilibrate at 4°C for 1 hour. The complex was loaded and run on a Superdex 200 (GE) Gel-filtration column.

SARS-CoV-2 spike pseudovirus infectivity experiments

SARS-CoV-2pp (2019-nCoV) was obtained from Cellecta Inc. (Catalog #RSCOV2-SL at 2.21×10^4 TU/ml). Infections were performed in 96-well plates. Pseudotyped viruses (10 μl per well) were incubated with serial dilutions of antibody for 1 hour at 37°C. Then the virus-antibody complex was used to infect 20,000 ACE2-expressing HEK293 cells (ATCC cat # CRL-1573) to a final volume of 100 μl. The mixtures were then incubated for 48 hours at 37°C in a humidified incubator with 5% CO_2. Luciferase activity was measured using the Bright-Glo reagent (Promega) according to the manufacturer's instructions. This reagent lyses cells and provides luciferase substrate, resulting in a luminescence signal that is proportional to luciferase expression. Because the pseudovirus encodes luciferase, luminescence after addition of Bright-Glo was used as a proxy for pseudovirus infection level.

Affinity maturation nanoswitch screen

The library for the affinity maturation screen was created similarly to the original naïve library, except the oligonucleotides corresponding to the three CDR regions were pooled oligonucleotides (oPool from IDT) of the collection of Nb1 sequences with "NNK" mutated into each amino acid codon in the CDR regions. Paired-end 300-bp sequencing was performed on a Next2000 P2 kit. Sequences for which the forward and reverse reads did not match were discarded. Because of the strength of Nb1, for fig. S10B, we did not use latching.

Screening for PPARγ agonists

The PPARγ screen was performed by a single round of bead-based prescreening followed by a nanoswitch screen. The single round of prescreening was as described for the SARS-CoV-2 screen above, except with protein concentrations of PPARγ at 1 μM and CBP-1 peptide at 5 μM. Also, instead of the mRNA display library, we used a 400 million commercially available DEL provided by HitGen (OpenDEL 3.1 sublibraries 003 and 029). The PPARγ nanoswitch screen was performed similarly to the β_2AR nanoswitch screen, except adapted to the commercially available DEL. To do this the capture sequence was designed with a region to bind to the nanoswitch, a PEG18 spacer for flexibility, and then a region to bind to the single-stranded region at the end of the DEL members. The nanoswitch enrichment experiment was performed over eight technical replicates. Analysis was performed using available code (*53*).

Validating PPARγ agonists

Ligand A (HitGen ID OpenDEL0029-205-82-52) and Ligand B (HitGen ID OpenDEL0029-78-297-423) were purchased from HitGen for validation experiments.

For the TR-FRET interaction assay between PPARγ and the co-activator peptide CBP-1, we used the LanthaScreen TR-FRET PPAR gamma Coactivator Assay Kit from Thermo Fisher. The experiment was performed according to the manufacturer's instructions with a final concentration of CBP-1 peptide of 500 nM.

For the cellular adipogenesis assay, we measured adipogenesis for OP9 cells (ATCC) following a previously established procedure (*54*). In brief, after 30,000 cells per well were grown to confluency, the cells were cultured for an additional 48 hours in growth media [minimum essential medium (MEM) alpha without ribonucleosides/deoxyribonucleosides supplemented with 20% fetal bovine serum and 1% penicillin and streptomycin], then media was replaced with the small molecule at the specified concentrations in a 0.1% DMSO vehicle diluted in differentiation media (growth media with 10% fetal bovine serum, 1% penicillin and streptomycin, 1.0 μg/ml human insulin, and 0.5 mM 3-isobutyl-1-methylxanthine). After 48 hours, media was replaced with the small molecule at the specified concentrations in adipocyte maintenance media (differentiation media without 3-isobutyl-1-methylxanthine). This maintenance media was replaced every 2 to 3 days until plates were assayed 7 days after induction of differentiation. Lipid uptake was measured using NucBlue to stain DNA and AdipoRed to stain lipids. The DNA content was used to normalize adipogenic activity by the cell count. All results were normalized to the maximal rosiglitazone response and to zero in the absence of any ligand.

Quantification and statistical analysis

Gel images were analyzed using a custom MATLAB program (*14*). For dose-response curves, the data are normalized to the looped intensities in the presence and absence of BI167107. The error is reported or shown as the standard error of the mean of the values calculated in at least three independent experiments.

REFERENCES AND NOTES

1. R. Santos *et al.*, A comprehensive map of molecular drug targets. *Nat. Rev. Drug Discov.* **16**, 19–34 (2017). doi: 10.1038/nrd.2016.230; pmid: 27910877
2. H. Rui, K. S. Ashton, J. Min, C. Wang, P. R. Potts, Protein–protein interfaces in molecular glue-induced ternary complexes: Classification, characterization, and prediction. *RSC Chem. Biol.* **4**, 192–215 (2023). doi: 10.1039/D2CB00207H; pmid: 36908699
3. L. Marques, N. Vale, Salbutamol in the management of asthma: A review. *Int. J. Mol. Sci.* **23**, 14207 (2022). doi: 10.3390/ijms232214207; pmid: 36430683
4. S. P. Marso *et al.*, Semaglutide and cardiovascular outcomes in patients with type 2 diabetes. *N. Engl. J. Med.* **375**, 1834–1844 (2016). doi: 10.1056/NEJMoa1607141; pmid: 27633186
5. M. Bacalhau *et al.*, Elexacaftor-tezacaftor-ivacaftor: A life-changing triple combination of CFTR modulator drugs for cystic fibrosis. *Pharmaceuticals* **16**, 410 (2023). doi: 10.3390/ph16030410; pmid: 36986509
6. A. Chacon, X. Leleu, A. Bobin, 30 years of improved survival in non-transplant-eligible newly diagnosed multiple myeloma. *Cancers* **15**, 1929 (2023). doi: 10.3390/cancers15071929; pmid: 37046589
7. L. M. Mayr, D. Bojanic, Novel trends in high-throughput screening. *Curr. Opin. Pharmacol.* **9**, 580–588 (2009). doi: 10.1016/j.coph.2009.08.004; pmid: 19775937
8. R. A. Goodnow Jr., C. E. Dumelin, A. D. Keefe, DNA-encoded chemistry: Enabling the deeper sampling of chemical space. *Nat. Rev. Drug Discov.* **16**, 131–147 (2017). doi: 10.1038/nrd.2016.213; pmid: 27932801
9. M. Pettersson, C. M. Crews, PROteolysis TArgeting Chimeras (PROTACs)—Past, present and future. *Drug Discov. Today. Technol.* **31**, 15–27 (2019). doi: 10.1016/j.ddtec.2019.01.002; pmid: 31200855
10. P. Yin, H. M. T. Choi, C. R. Calvert, N. A. Pierce, Programming biomolecular self-assembly pathways. *Nature* **451**, 318–322 (2008). doi: 10.1038/nature06451; pmid: 18202654
11. X. Wang, T. Ha, Defining single molecular forces required to activate integrin and notch signaling. *Science* **340**, 991–994 (2013). doi: 10.1126/science.1231041; pmid: 23704575
12. K. Pardee *et al.*, Paper-based synthetic gene networks. *Cell* **159**, 940–954 (2014). doi: 10.1016/j.cell.2014.10.004; pmid: 25417167
13. J. J. Funke *et al.*, Uncovering the forces between nucleosomes using DNA origami. *Sci. Adv.* **2**, e1600974 (2016). doi: 10.1126/sciadv.1600974; pmid: 28138524
14. M. A. Koussa, K. Halvorsen, A. Ward, W. P. Wong, DNA nanoswitches: A quantitative platform for gel-based biomolecular interaction analysis. *Nat. Methods* **12**, 123–126 (2015). doi: 10.1038/nmeth.3209; pmid: 25486062
15. P. C. Nickels *et al.*, Molecular force spectroscopy with a DNA origami-based nanoscopic force clamp. *Science* **354**, 305–307 (2016). doi: 10.1126/science.aah5974; pmid: 27846560

Downloaded from https://www.science.org at Harvard University on November 05, 2026

16. I. Ponzo *et al.*, Proximity binding assay for PROTAC ternary complex analysis. *ACS Sens.* **11**, 3876–3888 (2026). doi: 10.1021/acssensors.5c04944; pmid: 42011828
17. D. Kostrz *et al.*, A modular DNA scaffold to study protein-protein interactions at single-molecule resolution. *Nat. Nanotechnol.* **14**, 988–993 (2019). doi: 10.1038/s41565-019-0542-7; pmid: 31548690
18. D. Soukarié *et al.*, Single-molecule sandwich aptasensing on nanoarrays by tethered particle motion analysis. *Anal. Chem.* **94**, 4319–4327 (2022). doi: 10.1021/acs.analchem.1c04995; pmid: 35226451
19. Y. Wang *et al.*, Label-free single-molecule quantification of rapamycin-induced FKBP-FRB dimerization for direct control of cellular mechanotransduction. *Nano Lett.* **19**, 7514–7525 (2019). doi: 10.1021/acs.nanolett.9b03364; pmid: 31466449
20. K. Halvorsen, D. Schaak, W. P. Wong, Nanoengineering a single-molecule mechanical switch using DNA self-assembly. *Nanotechnology* **22**, 494005 (2011). doi: 10.1088/0957-4484/22/49/494005; pmid: 22101354
21. R. Doshi *et al.*, *In vitro* nanobody discovery for integral membrane protein targets. *Sci. Rep.* **4**, 6760 (2014). doi: 10.1038/srep06760; pmid: 25342225
22. L. Han *et al.*, Concentration and length dependence of DNA looping in transcriptional regulation. *PLOS ONE* **4**, e5621 (2009). doi: 10.1371/journal.pone.0005621; pmid: 19479049
23. A. S. Hauser, M. M. Attwood, M. Rask-Andersen, H. B. Schiöth, D. E. Gloriam, Trends in GPCR drug discovery: New agents, targets and indications. *Nat. Rev. Drug Discov.* **16**, 829–842 (2017). doi: 10.1038/nrd.2017.178; pmid: 29075003
24. D. P. Staus *et al.*, Allosteric nanobodies reveal the dynamic range and diverse mechanisms of G-protein-coupled receptor activation. *Nature* **535**, 448–452 (2016). doi: 10.1038/nature18636; pmid: 27409812
25. R. Irannejad *et al.*, Conformational biosensors reveal GPCR signalling from endosomes. *Nature* **495**, 534–538 (2013). doi: 10.1038/nature12000; pmid: 23515162
26. B. A. Kumar, P. Kumari, C. Sona, P. N. Yadav, GloSensor assay for discovery of GPCR-selective ligands. *Methods Cell Biol.* **142**, 27–50 (2017). doi: 10.1016/bs.mcb.2017.07.012; pmid: 28964338
27. Q. Wan *et al.*, Mini G protein probes for active G protein-coupled receptors (GPCRs) in live cells. *J. Biol. Chem.* **293**, 7466–7473 (2018). doi: 10.1074/jbc.RA118.001975; pmid: 29523687
28. S. C. Wright *et al.*, BRET-based effector membrane translocation assay monitors GPCR-promoted and endocytosis-mediated G_q activation at early endosomes. *Proc. Natl. Acad. Sci. U.S.A.* **118**, e2025846118 (2021). doi: 10.1073/pnas.2025846118; pmid: 33990469
29. S. G. F. Rasmussen *et al.*, Structure of a nanobody-stabilized active state of the β_2 adrenoceptor. *Nature* **469**, 175–180 (2011). doi: 10.1038/nature09648; pmid: 21228869
30. D. Weichert *et al.*, Covalent agonists for studying G protein-coupled receptor activation. *Proc. Natl. Acad. Sci. U.S.A.* **111**, 10744–10748 (2014). doi: 10.1073/pnas.1410415111; pmid: 25006259
31. D. Weichert, P. Gmeiner, Covalent molecular probes for class A G protein-coupled receptors: Advances and applications. *ACS Chem. Biol.* **10**, 1376–1386 (2015). doi: 10.1021/acschembio.5b00070; pmid: 25860503
32. Z. J. Gartner *et al.*, DNA-templated organic synthesis and selection of a library of macrocycles. *Science* **305**, 1601–1605 (2004). doi: 10.1126/science.1102629; pmid: 15319493
33. R. Seifert, "BRL37344" in *xPharm: The Comprehensive Pharmacology Reference*, S. J. Enna, D. B. Bylund, Eds. (Elsevier, 2008).
34. J. G. Baker, The selectivity of β-adrenoceptor agonists at human β_1-, β_2- and β_3-adrenoceptors. *Br. J. Pharmacol.* **160**, 1048–1061 (2010). doi: 10.1111/j.1476-5381.2010.00754.x; pmid: 20590599
35. B. Carpenter, R. Nehmé, T. Warne, A. G. W. Leslie, C. G. Tate, Structure of the adenosine A_{2A} receptor bound to an engineered G protein. *Nature* **536**, 104–107 (2016). doi: 10.1038/nature18966; pmid: 27462812
36. R. Nehmé *et al.*, Mini-G proteins: Novel tools for studying GPCRs in their active conformation. *PLOS ONE* **12**, e0175642 (2017). doi: 10.1371/journal.pone.0175642; pmid: 28426733
37. Y. Liu *et al.*, An infectivity-enhancing site on the SARS-CoV-2 spike protein targeted by antibodies. *Cell* **184**, 3452–3466.e18 (2021). doi: 10.1016/j.cell.2021.05.032; pmid: 34139176
38. D. Li *et al.*, *In vitro* and *in vivo* functions of SARS-CoV-2 infection-enhancing and neutralizing antibodies. *Cell* **184**, 4203–4219.e32 (2021). doi: 10.1016/j.cell.2021.06.021; pmid: 34242577
39. C. Muñoz-Fontela *et al.*, Animal models for COVID-19. *Nature* **586**, 509–515 (2020). doi: 10.1038/s41586-020-2787-6; pmid: 32967005
40. C. McMahon *et al.*, Yeast surface display platform for rapid discovery of conformationally selective nanobodies. *Nat. Struct. Mol. Biol.* **25**, 289–296 (2018). doi: 10.1038/s41594-018-0028-6; pmid: 29434346
41. C. Laffeber, K. de Koning, R. Kanaar, J. H. G. Lebbink, Experimental evidence for enhanced receptor binding by rapidly spreading SARS-CoV-2 variants. *J. Mol. Biol.* **433**, 167058 (2021). doi: 10.1016/j.jmb.2021.167058; pmid: 34023401
42. C. Forest-Nault *et al.*, Impact of the temperature on the interactions between common variants of the SARS-CoV-2 receptor binding domain and the human ACE2. *Sci. Rep.* **12**, 11520 (2022). doi: 10.1038/s41598-022-15215-5; pmid: 35798770
43. A. S. de Souza *et al.*, Molecular dynamics analysis of fast-spreading severe acute respiratory syndrome coronavirus 2 variants and their effects on the interaction with human angiotensin-converting enzyme 2. *ACS Omega* **7**, 30700–30709 (2022). doi: 10.1021/acsomega.1c07240; pmid: 36068861
44. V. Monteil *et al.*, Clinical grade ACE2 as a universal agent to block SARS-CoV-2 variants. *EMBO Mol. Med.* **14**, e15230 (2022). doi: 10.15252/emmm.202115230; pmid: 35781796
45. B. M. Spiegelman, PPAR-gamma: Adipogenic regulator and thiazolidinedione receptor. *Diabetes* **47**, 507–514 (1998). doi: 10.2337/diabetes.47.4.507; pmid: 9568680
46. H. Yki-Järvinen, Thiazolidinediones. *N. Engl. J. Med.* **351**, 1106–1118 (2004). doi: 10.1056/NEJMra041001; pmid: 15356308
47. S. Ahn *et al.*, Allosteric "beta-blocker" isolated from a DNA-encoded small molecule library. *Proc. Natl. Acad. Sci. U.S.A.* **114**, 1708–1713 (2017). doi: 10.1073/pnas.1620645114; pmid: 28130548
48. S. Ahn *et al.*, Small-molecule positive allosteric modulators of the β_2-adrenoceptor isolated from DNA-encoded libraries. *Mol. Pharmacol.* **94**, 850–861 (2018). doi: 10.1124/mol.118.111948; pmid: 29769246
49. L. Gu *et al.*, Multiplex single-molecule interaction profiling of DNA-barcoded proteins. *Nature* **515**, 554–557 (2014). doi: 10.1038/nature13761; pmid: 25252978
50. C. C. Forbes, K. M. DiVittorio, B. D. Smith, Bolaamphiphiles promote phospholipid translocation across vesicle membranes. *J. Am. Chem. Soc.* **128**, 9211–9218 (2006). doi: 10.1021/ja0619253; pmid: 16834395
51. W. Zeinyeh *et al.*, Synthesis and modulation properties of imidazo[4,5-*b*]pyridin-7-one and indazole-4,7-dione derivatives towards the *Cryptosporidium parvum* CpABC3 transporter. *Eur. J. Med. Chem.* **45**, 2480–2488 (2010). doi: 10.1016/j.ejmech.2010.02.033; pmid: 20207054
52. B. T. DeVree *et al.*, Allosteric coupling from G protein to the agonist-binding pocket in GPCRs. *Nature* **535**, 182–186 (2016). doi: 10.1038/nature18324; pmid: 27362234
53. R. Coffey, NGS-Barcode-Count, v0.11.1, GitHub (2023); https://github.com/Roco-scientist/NGS-Barcode-Count.
54. C. D. Kassotis *et al.*, Characterization of adipogenic chemicals in three different cell culture systems: implications for reproducibility based on cell source and handling. *Sci. Rep.* **7**, 42104 (2017). doi: 10.1038/srep42104; pmid: 28176856
55. C. H. Hansen *et al.*, Supporting Data for Discovering molecular modulators with nanoswitch screening, Zenodo (2026); https://doi.org/10.5281/zenodo.20385924.

ACKNOWLEDGMENTS

We thank members of the laboratory of W.P.W. for discussions. **Funding:** This work was supported by National Institutes of Health grant NIGMS R35 GM119537 (W.P.W.); an Arnold and Mabel Beckman Foundation, Beckman Young Investigator Award (W.P.W.); Takeda Pharmaceuticals (W.P.W.); a Smith Family Award for Excellence in Biomedical Research (A.C.K.); National Institutes of Health grant R01CA260415 (A.C.K.); National Institutes of Health grant NIGMS F31 GM128233 (S.C.E.); DFG Grant Gm 13/10 (P.G.); the Elite Network of Bavaria (T.S.); Boston Children's Hospital (W.P.W.); and Wyss Institute at Harvard (W.P.W., S.G.B.). This content is solely the responsibility of the authors and does not necessarily represent the official views of the National Institutes of Health. **Author contributions:** Conceptualization: C.H.H., A.C.K., W.P.W.; Performed experiments: C.H.H., M.L., S.C.E., T.S., S.G.B., A.C.K.; Performed analysis: C.H.H., W.P.W.; Supervision: P.G., A.C.K., W.P.W.; Writing – original draft: C.H.H., W.P.W.; Writing – review & editing: C.H.H., M.L., S.C.E., T.S., S.G.B., P.G., A.C.K., W.P.W. **Competing interests:** C.H.H. and W.P.W. have filed patent applications for various aspects of this work (e.g., 9,914,958 and 11,396,650). W.P.W. is a cofounder of Merge Bio Therapeutics. C.H.H. and M.L. are cofounders and now employees of Merge Bio Therapeutics. A.C.K. is a cofounder and consultant for biotechnology companies Tectonic Therapeutic and Seismic Therapeutic, and for the Institute for Protein Innovation, a nonprofit research institute. **Data, code, and materials availability:** All data are available in the manuscript or the supplementary materials or are deposited at Zenodo (*55*). Figure source data are provided in data S1. Materials are available from the authors upon reasonable request. **License information:** Copyright © 2026 the authors, some rights reserved; exclusive licensee American Association for the Advancement of Science. No claim to original US government works. https://www.science.org/about/science-licenses-journal-article-reuse

SUPPLEMENTARY MATERIALS

science.org/doi/10.1126/science.adt7185
Supplementary Text; Figs. S1 to S17; Tables S1 to S3; References (*56*–*60*);
MDAR Reproducibility Checklist; Data S1

Submitted 10 October 2024; resubmitted 28 February 2026; accepted 25 September 2026
10.1126/science.adt7185

Downloaded from https://www.science.org at Harvard University on November 05, 2026

Science
AAAS

Discovering molecular modulators with nanoswitch screening

Clinton H. Hansen, Mark Lipstein, Sarah C. Erlandson, Tobias Schwalbe, Sylvie G. Bernier, Peter Gmeiner, Andrew C. Kruse, and Wesley P. Wong

Science **394** (6824), eadt7185. DOI: 10.1126/science.adt7185

Editor's summary

Control mechanisms in cells often regulate interactions between two or more proteins. This offers an opportunity for drug discovery if one can screen for small molecules that alter such interactions. Hansen *et al*. developed a method that uses DNA nanoswitches to monitor interactions of very large libraries of proteins for effects on protein interactions. The method allowed detection of ligands for the human beta-2 adrenergic receptor that both bound the receptor and promoted G protein signaling. Similarly, the researchers selected a ligand from a library of 400 million compounds that bound the nuclear receptor peroxisome proliferator-activated receptor gamma (PPAR#) and enhanced association with a transcriptional coactivator target. The combination of rapid high-throughput screening with functional assessment shows potential to accelerate drug discovery. —L. Bryan Ray

View the article online
https://www.science.org/doi/10.1126/science.adt7185
Permissions
https://www.science.org/help/reprints-and-permissions

Downloaded from https://www.science.org at Harvard University on November 05, 2026

Use of this article is subject to the Terms of service

Science (ISSN 1095-9203) is published by the American Association for the Advancement of Science. 1200 New York Avenue NW, Washington, DC 20005. The title *Science* is a registered trademark of AAAS.

Copyright © 2026 The Authors, some rights reserved; exclusive licensee American Association for the Advancement of Science. No claim to original U.S. Government Works